

DTIC FILE COPY

4

AD-A219 215

GL-TR-89-0224

Regional Studies with Broadband Data

**Thomas V. McEvilly
Lane R. Johnson**

**University of California
Seismographic Station
Berkeley, CA 94720**

7 August 1989

**DTIC
ELECTE
MAR 12 1990
S D & D**

**Final Report
6 March 1988 - 5 June 1989**

APPROVED FOR PUBLIC RELEASE; DISTRIBUTION UNLIMITED

**GEOPHYSICS LABORATORY
AIR FORCE SYSTEMS COMMAND
UNITED STATES AIR FORCE
HANSCom AIR FORCE BASE, MASSACHUSETTS 01731-5000**

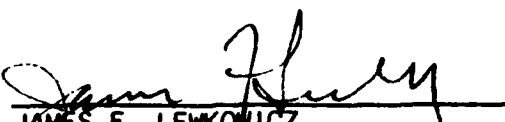
90 03 09 069

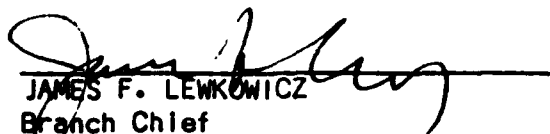
SPONSORED BY
Defense Advanced Research Projects Agency
Nuclear Monitoring Research Office
ARPA ORDER NO. 5299

MONITORED BY
Geophysics Laboratory
Contract No. F19628-87-K-0032


The views and conclusions contained in this document are those of the authors and should not be interpreted as representing the official policies, either expressed or implied, of the Defense Advanced Research Projects Agency or the U.S. Government.

This technical report has been reviewed and is approved for publication.


JAMES F. LEWKOWICZ
Contract Manager
Solid Earth Geophysics Branch
Earth Sciences Division


JAMES F. LEWKOWICZ
Branch Chief
Solid Earth Geophysics Branch
Earth Sciences Division

FOR THE COMMANDER


DONALD H. ECKHARDT, Director
Earth Sciences Division

This report has been reviewed by the ESD Public Affairs Office (PA) and is releasable to the National Technical Information Service (NTIS).

Qualified requestors may obtain additional copies from the Defense Technical Information Center. All others should apply to the National Technical Information Service.

If your address has changed, or if you wish to be removed from the mailing list, or if the addressee is no longer employed by your organization, please notify AFGL/DAA, Hanscom AFB, MA 01731-5000. This will assist us in maintaining a current mailing list.

Do not return copies of this report unless contractual obligations or notices on a specific document requires that it be returned.

REPORT DOCUMENTATION PAGE				Form Approved OMB No 0704-0188	
1a REPORT SECURITY CLASSIFICATION Unclassified			1b RESTRICTIVE MARKINGS		
2a SECURITY CLASSIFICATION AUTHORITY			3. DISTRIBUTION / AVAILABILITY OF REPORT Approved for public release Distribution unlimited		
2b DECLASSIFICATION / DOWNGRADING SCHEDULE					
4. PERFORMING ORGANIZATION REPORT NUMBER(S)			5 MONITORING ORGANIZATION REPORT NUMBER(S) GL-TR-89-0224		
6a NAME OF PERFORMING ORGANIZATION University of California		6b. OFFICE SYMBOL (If applicable)	7a. NAME OF MONITORING ORGANIZATION Geophysics Laboratory		
6c. ADDRESS (City, State, and ZIP Code) Geology and Geophysics University of California Berkeley, California 94720			7b. ADDRESS (City, State, and ZIP Code) Hanscom Air Force Base Massachusetts 01731-5000		
8a NAME OF FUNDING / SPONSORING ORGANIZATION DARPA		8b OFFICE SYMBOL (If applicable) DARPA/GSD	9 PROCUREMENT INSTRUMENT IDENTIFICATION NUMBER F19628-87-K-0032		
8c ADDRESS (City, State, and ZIP Code) 1400 Wilson Boulevard Arlington, Virginia 22209			10 SOURCE OF FUNDING NUMBERS		
			PROGRAM ELEMENT NO 61101E	PROJECT NO 7A10	TASK NO DA
11 TITLE (Include Security Classification) Regional Studies with Broadband Data					
12. PERSONAL AUTHOR(S) McEvelly, Thomas V., Johnson, Lane R.					
13a TYPE OF REPORT Final		13b TIME COVERED FROM 3/6/88 TO 6/5/89		14 DATE OF REPORT (Year, Month, Day) 1989 August 7	
15 PAGE COUNT 72					
16. SUPPLEMENTARY NOTATION					
17. COSATI CODES			18 SUBJECT TERMS (Continue on reverse if necessary and identify by block number) explosions, seismic waves, moment tensor (EG)		
FIELD	GROUP	SUB-GROUP			
19 ABSTRACT (Continue on reverse if necessary and identify by block number) An experiment was performed in which broadband waveform data were recorded by a seismic network surrounding a series of 8 chemical explosions in a quarry. The experiment is described and all of the waveform data are presented. A velocity model was obtained from the travel time readings and this was used to estimate moment rate tensors for 5 of the events which were single explosions. The results indicate simple source mechanisms for these single explosions, particularly the deeper events. The efficiency with which chemical energy is converted to seismic waves shows a strong dependence upon the depth of the source and this is caused primarily by a decrease in the corner frequency of the source time function as the source depth decreases. When scaled by the size of the explosion, the results for these small chemical explosions are in reasonable agreement with similar results for much larger nuclear explosions.					
20 DISTRIBUTION / AVAILABILITY OF ABSTRACT <input checked="" type="checkbox"/> UNCLASSIFIED / UNLIMITED <input type="checkbox"/> SAME AS RPT <input type="checkbox"/> DTIC USERS			21 ABSTRACT SECURITY CLASSIFICATION Unclassified		
22a NAME OF RESPONSIBLE INDIVIDUAL James F. Lewkowicz			22b TELEPHONE (Include Area Code) (617) 377-3028		22c OFFICE SYMBOL GL/LWH

TABLE OF CONTENTS

NEAR-SOURCE OBSERVATIONS OF QUARRY EXPLOSIONS	1
Introduction	1
Experiment	2
Data	3
Velocity Model	4
Analysis	5
Conclusions	10
References	11
Tables	12
Figures	18

Accession For	
NTIS CRA&I	<input checked="" type="checkbox"/>
DTIC TAB	<input type="checkbox"/>
Unannounced	<input type="checkbox"/>
Justification	
By	
Distribution /	
Availability Codes	
Dist	Avail and/or Special
A-1	



Near-Source Observations of Quarry Explosions

Lane R. Johnson and Michael A. Leonard

Center for Computational Seismology, Lawrence Berkeley Laboratory,
and Department of Geology and Geophysics,
University of California, Berkeley

ABSTRACT

An experiment was performed in which broadband waveform data were recorded by a seismic network surrounding a series of 8 chemical explosions in a quarry. The experiment is described and all of the waveform data are presented. A velocity model was obtained from the travel time readings and this was used to estimate moment rate tensors for 5 of the events which were single explosions. The results indicate simple source mechanisms for these single explosions, particularly the deeper events. The efficiency with which chemical energy is converted to seismic waves shows a strong dependence upon the depth of the source and this is caused primarily by a decrease in the corner frequency of the source time function as the source depth decreases. When scaled by the size of the explosion, the results for these small chemical explosions are in reasonable agreement with similar results for much larger nuclear explosions.

Introduction

This report describes some of the results which have emerged from a special experiment in which a series of chemical explosions detonated in a quarry were recorded with a near-source network of seismometers. One of the objectives is to compare the results of this experiment with results from similar experiments involving nuclear explosions and to determine if certain fundamental aspects of elastic wave generation by explosions can be more easily investigated with small controlled chemical explosions than with larger nuclear explosions.

The recording experiments at the quarry were very similar to experiments performed in the past for nuclear explosions at the Nevada Test Site, with all distances and depths scaled down by a factor of about 10 for the quarry experiments. This series of controlled experiments has several potential advantages over similar experiments that have been performed at the Nevada Test Site. The same network was used to record a series of different explosions, so the possibility exists that the separate effects of source, propagation, and recording site can be isolated. Three separate explosions were detonated at different depths in the same drilled hole, thus permitting a direct comparison of the

effects of source depth.

The main purpose of the present report is to describe the experiment and the data which it produced. Some preliminary estimates of the moment tensors for some of the source events are also presented. So far the analysis has been mainly concerned with the question of how the source mechanism of an explosion is affected by its depth. This particular set of experiments is well suited to an investigation of this affect.

Experiment

In the fall of 1988 a series of chemical explosions were detonated in the Kaiser Permanente Quarry near Menlo Park, California (37.32 deg N, 122.11 deg W). The explosions were arranged by Dr. Willie Lee of the U.S. Geological Survey. The U.S. Geological Survey deployed five different types of instruments over a broad area within and around the quarry and recorded a large number of data channels (Lee and Gibbs, 1989). The University of California's part of the experiment was to record broadband waveform data at a network of stations close to the explosions at distances within a few depths-of-burial.

The experiment consisted of ten different explosive events, including single explosions at various depths in drilled holes, regular quarry blasts consisting of simultaneous explosions in clusters of shallow drilled holes, and one event which was a combined quarry blast and single explosion in a drilled hole with both fired at about the same time. Table 1 contains information on the locations and sizes of the explosions. The accuracy of the origin times is better than 0.03 sec. The locations have a relative accuracy of about 1 meter. The elevation and depth both refer to the middle of the explosive material, with elevation being referenced to sea level and the depth being referenced to the surface at the drilled hole.

Two different types of events were involved in the experiment, a single explosion in a drilled hole and a quarry blast. For the purposes of this study a quarry blast is defined as a cluster of explosions in separate shallow drilled holes detonated at approximately the same time. Note that events KQ1, KQ3, and KQ5 were single explosions which were all detonated in the same drilled hole. Also note that event KQ10 was a combination of a quarry blast and a single explosion which were slightly separated in both time and space.

The recording network which collected the data used in this study consisted of 11 triggered digital event recorders. The sensors were three-component force-balance accelerometers. The data were digitized at 200 samples per second with a resolution of 12 bits per sample and the complete system response was flat to acceleration between frequencies of 0.2 and 50 Hz.

The same network was used to record all events in the experiment. The locations of the stations in the network are listed in Table 2 and plotted in Figure 1. Also shown in Figure 1 are the locations of the explosions of Table 1, with the exception of events KQ6 and KQ7. Both of these latter events were located outside the boundary of the recording network, so data from these events were not included in the study. The stations of the network were

distributed more or less uniformly over an area of slightly less than 1 square km, and for all of the events there was at least one station within 250 meters of the epicenter which produced usable data.

Because the experiment was conducted in a large quarry, the topographic relief was considerable. Table 2 shows that the maximum elevation change across the network was about 150 meters. All of the explosions used in this study and stations UCB1 through UCB6 of the network were located within the quarry and at approximately the same elevation, with event KQ9 and station UCB6 being slight exceptions, having smaller elevations than the rest. In contrast to this, stations UCB7 through UCB11 of the network were located outside the quarry on its rim and had elevations which average about 70 meters greater than the stations within the quarry.

Data

As mentioned above, only the data which were collected from the 8 events which were located within the recording network are included in this report. Due to a variety of malfunctions, usable data were not obtained from all of the recording stations for all of these 8 events, with the number of stations producing usable data ranging between 5 and 11. A total of 198 usable seismograms were obtained from the 8 events.

The waveform data which were recorded from the 8 events are shown in Figures 2 through 25. Relative locations of the stations with respect to these 8 events can be found in Tables 3 through 10. In Tables 3-10 the range column denotes horizontal distance from epicenter to receiver, while the distance column denotes slant distance from hypocenter to receiver. In Figures 2-25 the seismograms have been arranged in order of increasing range and scaled by multiplying each seismogram by its range. Zero time corresponds roughly to the detonation of the explosion. Because of differences in elevation of the recording stations, an ordering in terms of range is not always an ordering in terms of distance, and thus first arrival times are not always monotonic in range.

In preparing Figures 2-25 and Tables 3-10 the horizontal components of acceleration were rotated to form a radial component (positive away from the source) and a transverse component (positive clockwise about the source as viewed from above). The vertical component is positive up. Also included in the tables are the maximum accelerations measured from the waveforms.

Several general observations apply to the entire data set. The first arriving signal always has a sense of first motion which is up and away from the source, which is what one expects from an explosive source below the receiver. Note that this is even true for station UCB6, which is at a lower elevation than events KQ2, KQ4, KQ5, KQ8, and KQ10a, indicating that in its path from source to receiver the first arriving energy has followed a curved path and penetrated to a lower elevation than that of the receiver. This is to be expected if the velocity increases with depth. In almost all cases the first arrival has larger amplitudes on the vertical than the radial component, and this pattern is most pronounced for the deeper events and for the stations at higher elevations.

On the transverse components the first discernible motion begins at the same time as on the vertical and radial components, but in general it is more emergent and the direction of first motion changes from station to station. However, before the first cycle is completed the amplitude on the transverse component has usually grown to a value comparable to that on the radial component.

The fact that event KQ10 consists of two separate sources is clearly evident in Figures 23-25. The waves from the shallow quarry blast are much smaller in amplitude than those from the deeper single explosion which begin about 0.15 sec later. This is in spite of the fact that the total amount of explosive in the quarry blast is much larger than that in the single explosion (see Table 1).

Some of the advantages of using the same network to record a series of different sources are readily evident in the waveform data. For instance, for all of the events station UCB3 seems to have anomalously large amplitudes compared to other stations at about the same distance. This observation applies to all three components and suggests the existence of local features near this station which causes an amplification of the seismic waves. In principle, station amplification factors such as this could be extracted from the data set itself using a least-squares procedure. Knowledge of such factors could be very useful in the analysis of the data.

The data set is particularly well suited for studies of how the depth of a source affects the elastic waves it radiates. This is because the data set contains records from 3 different explosions of about the same size detonated at different depths in the same drilled hole: KQ01, KQ03, and KQ05. The depths (and sizes) of the explosions were 217 meters (1000 pounds), 106 meters (900 pounds), and 42 meters (900 pounds) (see Table 1). A comparison of the accelerations from the deep and intermediate explosions (compare Figure 2 with 8, Figure 3 with 9, and Figure 4 with 10) shows few differences with similar waveforms and slightly reduced amplitudes for the intermediate depth explosion. However, when the deep or intermediate event is compared with the shallow event (compare Figure 2 or 8 with 14, Figure 3 or 9 with 15, and Figure 4 or 10 with 16), much more dramatic differences are observed. The accelerations from the shallow event are much reduced in amplitude at all distances (note the factor of 5 difference in the scale of the plots for the shallow event) and the seismograms have the general appearance of being more prolonged in time.

Velocity Model

The seismograms in Figures 2-25 represent the combined effects of both source and propagation. One of the objectives of this study is isolate the source effect, and a way of doing this is to solve for the force-moment tensor which represents the source. However, this requires the calculation of Green functions and this in turn requires that a velocity model be available. Thus one of the first steps in the analysis was to estimate a velocity model appropriate for the shallow part of the quarry where the seismic waves were propagating.

The velocity model for P-waves was estimated from the travel times of the first arrivals from the three events in the same drilled hole, KQ01, KQ03, and KQ05. These travel times are listed in Table 11. The inverse problem of converting these travel times to a velocity model is somewhat different from that usually encountered in seismology in that the large variation in the elevation of the receivers must be taken into account. The problem was solved by using a program which had been developed for estimating velocity structure and locating earthquakes using data from a borehole array. The problem under consideration here is actually easier because the locations of the sources are known and can be fixed at the outset. The basic procedure followed by the program is to linearize the problem and perturb the velocity through a series of damped iterations until the travel time residuals are minimized in a least squares sense. At this stage of the analysis it was decided to solve for the average one-dimensional velocity model which only varies in the vertical direction.

Figure 26 shows the one-dimensional P-wave velocity model for the limestone rocks of the quarry in the vicinity of the experiment which was estimated using procedure described above. The S velocity was obtained from the P velocity by assuming a constant Poisson's ratio of 0.25. Note that the shallow explosion (denoted by the number 5 in Figure 26) is in the part of the model where there are steep near-surface velocity gradients, while the two deeper explosions are in a part of the model where the velocity gradients are more gentle. In this respect, the shallow event is similar to nuclear explosions at Pahute Mesa which are above the water table, while the two deeper events are similar to events which are below the water table.

Analysis

So far the data from this experiment have been analyzed mainly in terms of the effect which source depth has upon the explosion mechanism. The basic idea is to compare sources which are similar except for their depth. While a certain amount of analysis of this type can be accomplished by comparing the seismograms themselves, it is generally more useful to remove the effects of propagation in order to allow more direct comparisons of the sources. A convenient way of performing this latter process is to estimate the force-moment tensor of the source, and preliminary results of this type have been calculated for 5 of the events.

Given seismograms recorded on a network surrounding the source and given a model of the velocity structure, it is fairly straightforward to estimate the second-order force moment tensor of the source. At the distances involved in this experiment the seismograms are fairly complex and contain overlapping contributions from near-field terms, P-waves, S-waves, Rayleigh waves, and Love waves. Thus the Green functions used in the moment tensor inversions must be fairly complete and contain all of these different parts of the solution. These can be obtained for one-dimensional models using standard propagator methods, although the computations are quite lengthy.

The considerable variation in topography across the recording network presents a special problem for the calculation of the Green functions, since it

represents a departure from a one-dimensional structure. A compromise solution to this problem was attempted by calculating Green functions for two different models of the quarry velocity structure, one having a free surface at an elevation of 360 meters and the other having a free surface at an elevation of 430 meters (see Figure 26). The first model was used for the stations within the quarry, UCB1-6, and the second model was used for stations outside the quarry, UCB7-11.

In representing the source in terms of its second-order force moment tensor the assumption is implied that the dimensions of the source are small compared to the wavelengths of interest. For a frequency of 50 Hz the S waves used in this study have wavelengths of about 20 meters. For the events in the experiment consisting of single explosions, the assumption that the source is small compared to this length seems to be reasonable. However, for the events which were quarry blasts this assumption becomes more suspect. It is definitely not valid for event KQ10 (see Figure 1) and it needs further study for events KQ02 and KQ04. For this reason, this report contains only the results of moment tensor inversions for the events which were single explosions.

The moment rate tensors that were estimated for the 5 events which were single explosions, KQ01, KQ03, KQ05, KQ08, and KQ09, are shown in Figures 27-31, respectively. The source depths for these events ranged between 10 and 217 meters and the explosion size ranged between 300 and 1000 pounds.

A few general observations apply to all of the moment tensor results. In all cases the shape and polarity of the signal is quite similar on the three diagonal elements of the moment rate tensor, and the size of the signal on these elements is larger than on the off-diagonal elements. This result implies a source mechanism which involves a spherically symmetric change in volume, which agrees with the simple model of an explosive source as a pressure pulse on the interior of a spherical cavity. The two deepest sources (KQ01 in Figure 27 and KQ03 in Figure 28) have particularly simple moment rate tensors, consisting primarily of a single concentrated one-sided pulse beginning at the origin time on only the diagonal elements. This corresponds to a moment tensor consisting of a simple step having a rise time of about 0.03 second. The moment rate tensor for the shallower events are more complicated, with the initial pulse still present but less well defined on the diagonal elements at the origin time, and this is followed by other longer period signals which are generally in phase on the diagonal elements and smaller with more random phase on the off-diagonal elements.

The moment-rate tensor estimated for event KQ08 (Figure 30) is the most complicated. The initial pulse on the diagonal elements is slightly noncausal and of longer duration with the suggestion that it may consist of two or more pulses. While it may be that this source was actually more complicated than the others, there are other possible causes that must be considered. For the purposes of the moment tensor inversion the distribution of recording stations for this event was much worse than for the other events, with only 15 components included in the inversion and all of these contributed by stations located in the same azimuthal quadrant. Thus, this moment-rate tensor is judged to be the

most poorly determined of the 5.

A simple explosion consisting of a spherically symmetric change in volume should have a moment tensor with only an isotropic part and a zero deviatoric part. Here the isotropic part is taken to be one third the trace of the moment tensor. As pointed out above, the estimated moment rate tensors are all dominated by their diagonal elements and the signals on these diagonal elements are quite similar in both their shape and polarity. This means that the isotropic part of the moment tensor is much larger than the deviatoric part, and this is consistent with expectations for a simple explosion. Thus the isotropic parts of the moment rate tensors can be used as a representation of the explosive part of the source mechanism.

The isotropic parts of the moment rate tensors shown in Figures 27-31 were calculated and their Fourier transforms computed to obtain the spectra shown in Figures 32-36 for the events KQ01, KQ03, KQ05, KQ08, and KQ09, respectively. All of these spectra are similar in that they have relatively flat sections at low frequencies and steep decaying sections at high frequencies. The low frequency levels of these spectra were measured in the 5-10 Hz range and these are listed in Table 12. The high frequency asymptotes were extrapolated back to where they intersected the low frequency levels and these were used as estimates of the corner frequencies, which are also listed in Table 12. Also shown in Table 12 are the maximum values of the isotropic parts of the moment rate tensors as measured in the time domain, with this maximum occurring in most cases during the pulse which begins at the origin time.

The spectra of isotropic moment rate tensors shown in Figures 32-36 and the summary values in Table 12 show some interesting differences. The deeper events, KQ01 and KQ03, are relatively flat out to corner frequencies between 30 and 40 Hz. In fact, the corner frequency for event KQ01 is close enough to the corner frequency of the anti-alias filter at 50 Hz so that part of the roll off at high frequencies in Figure 32 may be caused by the recording system. The spectra for the shallower events are considerably depleted in the higher frequencies in comparison to the deeper events. For event KQ05 and KQ08 the corner frequencies are at about 10 Hz. Interpreting the spectra of event KQ09 is more problematical, with a peak in the spectra near 10 Hz and what appears to be a corner frequency at about 26 Hz. It should be emphasized that estimates of spectral characteristics such as those listed in Table 12 are rather subjective and must be used with caution. It is more meaningful to make direct comparisons of the spectra than to compare estimates of the spectral characteristics.

As mentioned above, the three events at different depths in the same drilled hole (KQ01, KQ03, and KQ05) provide a well controlled test of the effects of source depth upon an explosive source. The moment rate tensors for these three events (Figures 27, 28, and 29) exhibit the same pattern which was observed in the seismograms. The two deeper events are quite similar in both the shape and amplitude of the time dependence of the moment rate tensors. However, the shallow event shows significant differences from the other two, with smaller maximum amplitudes, a less distinct pulse at the origin time, and relatively more energy at later times. Comparing the maximum isotropic

moment rate tensors in the time domain (Table 12) shows an almost linear dependence upon source depth. Recalling that the size of the three explosions differ by only 10%, these results indicate that the efficiency with which chemical energy is converted to seismic waves is strongly affected by source depth.

Additional information about the effects of source depth can be found in the spectra of the isotropic moment rates. Figure 37 compares on the same plot these spectra for the three events in the same drilled hole. The point of interest here is that, while the three explosions have similar spectral levels for frequencies less than 10 Hz, they differ considerably at higher frequencies. In particular, the deep and intermediate explosions have relatively flat spectra out to corner frequencies beyond 30 Hz, while the spectrum of the shallow explosion is markedly deficient in higher frequencies, with a corner frequency which is less well defined, but near 10 Hz. However, regardless of any estimates of corner frequencies, there is little question that the three spectra are quite similar below 10 Hz but show marked differences above 10 Hz which appear to be related to source depth. These results are entirely consistent with the differences that were noted above with regard to maximum accelerations on the seismograms and the maximum values of the time domain isotropic moment rates. It is also worth noting that the effects of source depth observed in this study are similar to those observed by Flynn and Stump (1988) for small chemical explosions detonated at a range of depths in dry alluvium.

In this study the method of moment tensor inversion appears to have been successful in removing most of the effects of wave propagation between source and receiver and thus allowing a more direct examination of the source mechanism. The results thus obtained seem to show that the source mechanism is strongly dependent upon source depth. However, it is possible that the efficiency of the inversion process could depend upon the depth of the source in such a way that differences in the results that appear to be related to the source depth may have been introduced in the process of doing the inversion. Such reasoning is made plausible by the fact that the accuracy of the inversion process is directly related to the accuracy of the Green functions, and these may be less accurate for shallow sources where scattering from near surface three-dimensional inhomogeneities is likely to be more significant.

An independent check upon the validity of the moment tensor results can be obtained from the seismograms themselves. Figure 38 shows the first arriving P wave at the same station for the three explosions in the same drilled hole. The waveforms have similar shapes, although the pulse from the shallow event seems to be composed of slightly longer periods. Note that the maximum amplitude of this pulse actually decreases as the distance from the source decreases, even though one would predict the opposite effect solely on the basis of geometrical spreading and attenuation. The reasons for these differences are further clarified in Figure 39, which compares the spectra of these pulses for the shallow and deep events. The spectrum of the intermediate event is very similar to that of the deep event. Note that the spectra are quite similar for frequencies below 10 Hz, but at higher frequencies the shallow event becomes increasingly deficient in energy, falling off by a factor of about 10 by 30 Hz.

These results are almost identical to those shown in Figure 37, and thus confirm the general pattern observed in the moment rate tensor.

The results from the three events in the same drilled hole suggest a couple of simple empirical generalizations about the effect of source depth upon the explosive source mechanism. First, the low frequency level of the isotropic moment rate spectrum is unaffected by source depth and is related to the size of the explosion. Second, the corner frequency is directly related to the source depth and decreases as the source depth decreases.

The results for the other two single explosion events, KQ08 and KQ09, seem to be consistent with these generalizations. The low frequency levels of their isotropic moment rate tensors are similar to each other but a factor of 2-3 less than for the larger events KQ01, KQ03, and KQ05 (see Figures 35 and 36 and Table 12). This ratio is in reasonable agreement with the relative sizes of the explosions.

The corner frequencies of the isotropic moment rate tensors for events KQ08 and KQ09 are also consistent with the results for the other three single explosions if the comparison is made with respect to the relative elevations of the events rather than the depths below the surface at the location of the event. Thus in Table 12 event KQ08 has the lowest corner frequency and the largest elevation, while event KQ09 has an elevation in between KQ03 and KQ05 and its corner frequency also falls in between the values for these events. This result suggests that the corner frequency is more affected by the material properties in the source region than by its depth below the surface. If this were so and assuming the model shown in Figure 26 is reasonable and material properties are primarily a function of elevation, then one would expect an apparent dependence upon source elevation or a somewhat more ambiguous apparent dependence upon source depth.

This last suggestion that material properties are actually the controlling factor in determining the corner frequencies is supported by the observation that events KQ01, KQ03, and KQ09 all have corner frequencies above 25 Hz and are all located at lower elevations where the velocity is high and the velocity gradient is low, while the events KQ05 and KQ08 which have corner frequencies lower than 10 Hz are located at the higher elevations where the velocity is low and the velocity gradient is high (see Figure 26). It should be noted that for sake of this discussion, ambient stress is considered to be a material property.

Finally, it is of interest to compare the scaled results for the chemical explosions of this study with similar results for nuclear explosions. Such a comparison is facilitated by converting the low frequency level of the isotropic moment rate tensor to the long time response of the reduced displacement potential Ψ_{∞} (see Johnson, 1988, for details). Then letting W be the size of the explosion in kilotons of TNT, the results shown in Figure 40 are obtained. Note that in order to have a consistent depth in this plot, the depths used for events KQ08 and KQ09 were measured from the top of the drilled hole containing the other three events. These results show that for the five single explosion events of this study there is a fairly linear relationship between the scaled

long time response of the reduced displacement potential and the scaled depth. According to simple theory, the long time reduced displacement potential is proportional to the effective volume of the source. Thus these results indicate that the effective source volume increases as the source depth decreases. This is consistent with an explanation in terms of decreased overburden pressure and/or weaker materials at shallower depths.

Also shown in Figure 40 for comparison are two different scaling relationships which were derived from nuclear explosion data. The scaling relationship of Mueller and Murphy (1971) is partly analytical and partly empirical and is appropriate for large nuclear explosions in a saturated tuff-rhyolite source medium. The Helmberger-Hadley scaling relationship is taken from Barker et al. (1985) and is appropriate for the same type of source medium. An interesting aspect of Figure 40 is that the scaled results from this study exhibit a relative trend that agrees well with both of the scaling relationships developed for nuclear explosions and also have absolute values that approximately split the difference between the two scaling relationships.

Figure 40 also contains scaled results from two nuclear explosions taken from Johnson (1988). The sizes of these explosions were estimated from body wave magnitudes using an equation from Aki et al. (1974). This gave values of 107 Kt for Harzer and 78 Kt for Chancellor. The Ψ_0 values were taken from Johnson (1988) and were obtained by the same type of moment tensor inversions used in this study. The predictions of the Mueller-Murphy and Helmberger-Hadley scaling relationships are also shown for these nuclear events. Note that the relative agreement between the scaled moment tensor results and the published scaling relationships is about the same for both the nuclear explosions and the chemical explosions, even though the difference in their sizes is over 5 orders of magnitude. It seems noteworthy that, although the two published scaling relationships were developed specifically to explain large nuclear explosions, they do almost as well in explaining the small chemical explosions. This seems to suggest that the some of the same physical processes are involved in these two kinds of explosions. Finally, note that, in comparison to the nuclear explosions, the scaled depths of the single explosions of this study are considerably over buried.

Conclusions

These controlled experiments with chemical explosions have indicated that source depth may significantly affect the efficiency with which explosions generate elastic waves. Furthermore, this effect seems to be strongly frequency dependent. The results generated so far must still be regarded as preliminary, but they have suggested several interesting questions which will have to be examined in future analysis. A critical question is to determine what physical processes are actually controlling this apparent source depth effect. A better understanding of these processes should be helpful in attributing the depth effect to the relevant physical parameters, such as overburden pressure, density, elasticity, or porosity.

An impression acquired from the analysis completed so far is that, with respect to the recorded waveforms and the estimated moment tensors, these small chemical explosions seem to exhibit similar characteristics to large nuclear explosions. However, the experiments with the chemical explosions are much easier to perform. In particular, the potential for isolating and studying a particular phenomenon through a series of carefully controlled experiments is much higher for the chemical explosions. Thus, the study of small chemical explosions offers an attractive approach to investigating some of the remaining problems associated with the generation of elastic waves by nuclear explosions.

References

- Aki, K., M. Bouchon, P. Reasenberg, Seismic source function for an underground nuclear explosion, *Bull. Seism. Soc. Am.*, 64, 131, 1974.
- Barker, J. S., L. J. Burdick, T. C. Wallace, Analysis of near-field seismic waveforms from underground nuclear explosions, Scientific Report No. 1, AFGL-TR-85-0321, Woodward-Clyde Consultants, Pasadena, 126 pages, September 15, 1985, ADA165227.
- Flynn, E. C., B. W. Stump, Effects of source depth on near-source seismograms, *J. Geophys. Res.*, 93, 4820-4834, 1988.
- Johnson, L. R., Source characteristics of two underground nuclear explosions, *Geophys. J.*, 95, 15-30, 1988.
- Lee, W. H. K., and J. F. Gibbs, Kaiser Quarry source experiment, Preliminary report on data recorded by GEOS stations, U.S. Geological Survey, Menlo Park, 112 pages, February 11, 1989.
- Mueller, R. A., J. R. Murphy, Seismic characteristics of underground nuclear detonations, Part I. Seismic spectrum scaling, *Bull. Seism. Soc. Am.*, 61, 1675-1692, 1971.

Table 1. Shot Information for the 1988 Kaiser Quarry Experiment

Event	Date	OriginTime h:m:s	Latitude deg N	Longitude deg E	Elevation m	Depth m	Explosive pounds
KQ1	Oct 27	18:15:00.01	37.32397	122.10725	136	217	1,000
KQ2	Oct 27	18:30:16.42	37.32182	122.10890	320	10	7,000/14 holes
KQ3	Oct 28	18:15:00.01	37.32397	122.10725	245	106	900
KQ4	Oct 28	18:30:00.22	37.32347	122.10748	335	10	1,900/4 holes
KQ5	Oct 31	19:15:00.01	37.32397	122.10725	311	42	900
KQ6	Oct 31	19:30:00.16	37.31998	122.11247	320	10	640
KQ7	Oct 31	19:45:03.35	37.32213	122.12993	525	20	1,510
KQ8	Oct 31	19:46:00.16	37.32377	122.10752	335	10	340
KQ9	Nov 1	19:15:00.01	37.32015	122.11037	293	12	300
KQ10a	Nov 1	19:30:00.81	37.32408	122.10752	348	10	11,900/23 holes
KQ10b		19:30:00.91	37.32380	122.10707	272	81	1,000

Table 2. Locations of Seismic Recording Stations

Station	Latitude deg N	Longitude deg E	Elevation m
UCB1	37.32357	122.11045	366
UCB2	37.32264	122.11182	366
UCB3	37.32190	122.10810	352
UCB4	37.32045	122.10759	357
UCB5	37.31860	122.10723	360
UCB6	37.32016	122.11079	306
UCB7	37.32351	122.10526	428
UCB8	37.32493	122.10896	435
UCB9	37.32455	122.11141	454
UCB10	37.32115	122.10524	421
UCB11	37.32076	122.10321	404

Table 3. Maximum Accelerations from Event KQ1

Station	Azimuth deg E of N	Range m	Distance m	max R cm/sec**2	max T cm/sec**2	max Z cm/sec**2
UCB7	106	183	345	134	132	329
UCB8	305	186	352	115	72	264
UCB3	198	241	324	197	170	393
UCB1	261	287	368	53	94	112
UCB10	150	359	458	35	46	140
UCB9	280	374	491	59	54	185
UCB4	184	392	450	37	43	117
UCB2	250	431	489	70	123	137
UCB11	135	505	572	26	18	62
UCB6	217	526	553	25	35	34
UCB5	180	596	637	31	57	79

Table 4. Maximum Accelerations from Event KQ2

Station	Azimuth deg E of N	Range m	Distance m	max R cm/sec**2	max T cm/sec**2	max Z cm/sec**2
UCB3	82	72	79	401	287	479
UCB4	143	191	195	58	58	60
UCB6	222	249	249	37	41	23
UCB2	290	275	279	17	21	39
UCB8	359	345	364	19	16	11
UCB9	324	376	399	7	6	8
UCB5	157	387	389	16	15	23
UCB11	103	518	525	9	9	9

Table 5. Maximum Accelerations from Event KQ3

Station	Azimuth deg E of N	Range m	Distance m	max R cm/sec**2	max T cm/sec**2	max Z cm/sec**2
UCB8	305	186	266	102	66	195
UCB3	198	241	264	183	200	293
UCB1	261	287	311	51	63	91
UCB10	150	359	400	23	32	113
UCB9	280	374	428	59	41	159
UCB4	184	392	408	36	42	88
UCB2	250	431	448	28	31	36
UCB11	135	505	529	23	14	48
UCB6	217	526	529	21	39	27
UCB5	180	596	607	27	42	14

Table 6. Maximum Accelerations from Event KQ4

Station	Azimuth deg E of N	Range m	Distance m	max R cm/sec**2	max T cm/sec**2	max Z cm/sec**2
UCB3	197	182	183	94	74	106
UCB8	321	208	231	21	23	22
UCB1	272	263	265	17	14	10
UCB10	142	324	335	14	14	26
UCB4	181	335	336	20	8	21
UCB11	128	483	488	8	9	7

Table 7. Maximum Accelerations from Event KQ5						
Station	Azimuth deg E of N	Range m	Distance m	max R cm/sec**2	max T cm/sec**2	max Z cm/sec**2
UCB8	305	186	223	55	44	72
UCB3	198	241	244	64	50	90
UCB10	150	359	375	13	10	31
UCB9	280	374	400	9	11	14
UCB4	184	392	395	16	16	27
UCB2	250	431	434	8	8	11
UCB11	135	505	513	6	6	15
UCB6	217	526	526	8	10	10
UCB5	180	596	598	11	18	8

Table 8. Maximum Accelerations from Event KQ8						
Station	Azimuth deg E of N	Range m	Distance m	max R cm/sec**2	max T cm/sec**2	max Z cm/sec**2
UCB3	194	213	214	35	27	43
UCB10	145	353	363	10	6	8
UCB4	181	367	368	8	4	6
UCB6	216	494	495	3	3	2
UCB11	131	507	512	4	3	3

Table 9. Maximum Accelerations from Event KQ9

Station	Azimuth deg E of N	Range m	Distance m	max R cm/sec**2	max T cm/sec**2	max Z cm/sec**2
UCB4	90	246	254	22	21	42
UCB3	51	258	265	72	31	102
UCB2	332	275	285	72	49	72
UCB5	126	346	352	27	20	12
UCB10	80	461	478	8	8	21
UCB9	349	464	491	14	9	17
UCB11	89	635	645	6	7	19

Table 10. Maximum Accelerations from Event KQ10

Station	Azimuth deg E of N	Range m	Distance m	max R cm/sec**2	max T cm/sec**2	max Z cm/sec**2
UCB8	306	159	181	115	165	160
UCB7	107	210	225	140	147	341
UCB3	192	247	247	171	182	234
UCB9	278	349	365	25	21	51
UCB10	148	382	389	26	28	80
UCB4	181	404	404	32	40	52
UCB2	247	413	413	25	29	27
UCB6	214	523	525	25	38	38
UCB11	134	530	533	20	14	51
UCB5	177	609	609	29	39	29

Table 11. Travel Times of First Arrivals

Station	KQ01 sec	KQ03 sec	KQ05 sec
UCB7			
UCB8	.141	.121	.116
UCB3	.116	.101	.101
UCB1	.131	.116	
UCB10	.166	.151	.151
UCB9	.186	.176	.166
UCB4	.136	.131	.121
UCB2	.166	.151	.146
UCB11	.196	.191	.186
UCB6	.156	.146	.146
UCB5	.191	.181	.176

Table 12. Properties of Isotropic Moment Rates

Event	Elev. m	Depth m	Explosive pounds	Max. Time Domain 10**20 dyne cm/sec	Low Freq. Level 10**18 dyne cm	Corner Freq. Hz
KQ01	136	217	1000	1.56	2.37	37
KQ03	245	106	900	0.81	1.78	32
KQ05	311	42	900	0.31	1.99	11
KQ08	335	10	340	0.09	0.79	10
KQ09	293	12	300	0.28	0.75	26

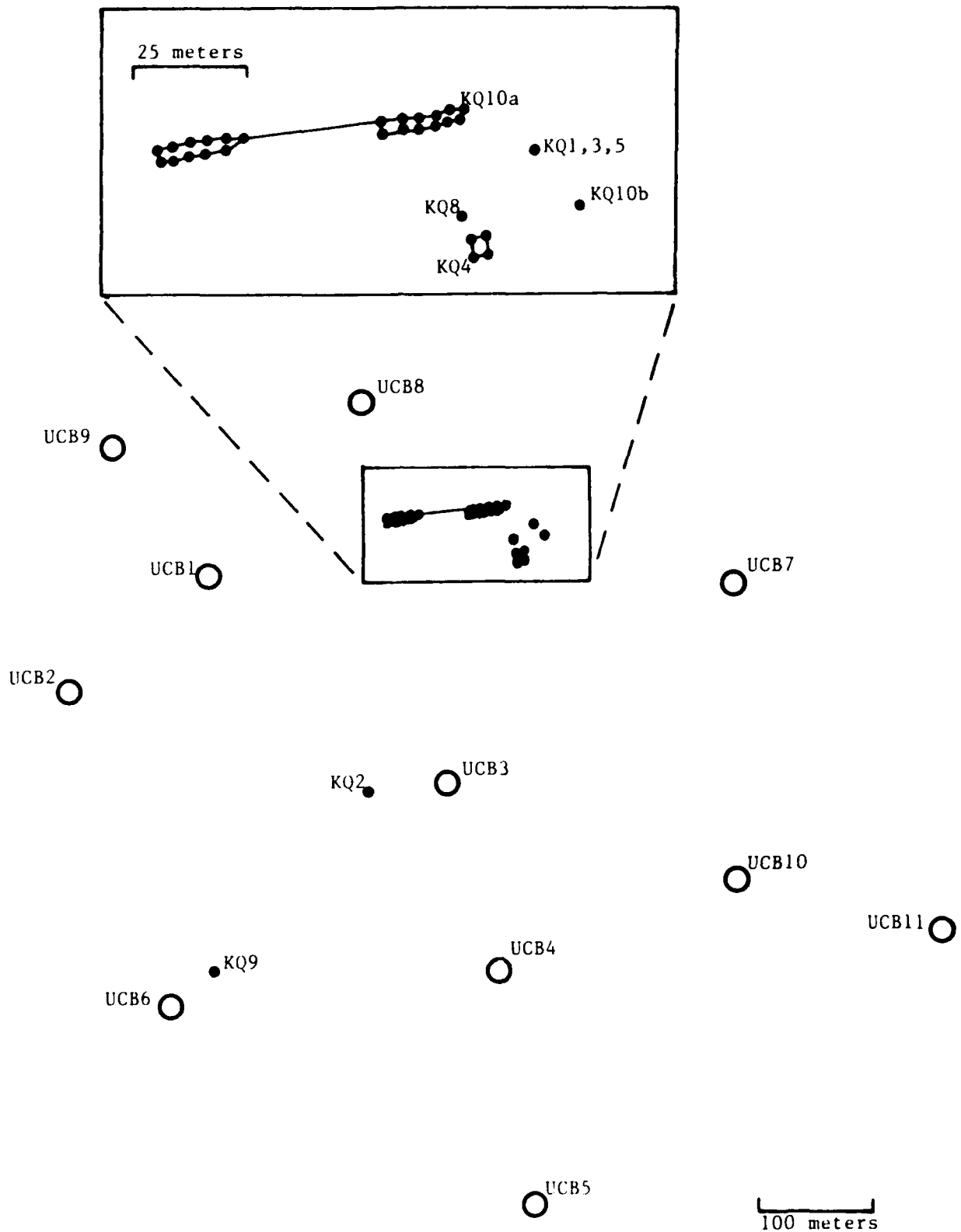


Figure 1. Map showing the location of the recording stations (UCB1 - UCB11) and the location of the explosions (KQ1 - KQ10) at the Kaiser Permanente Quarry.

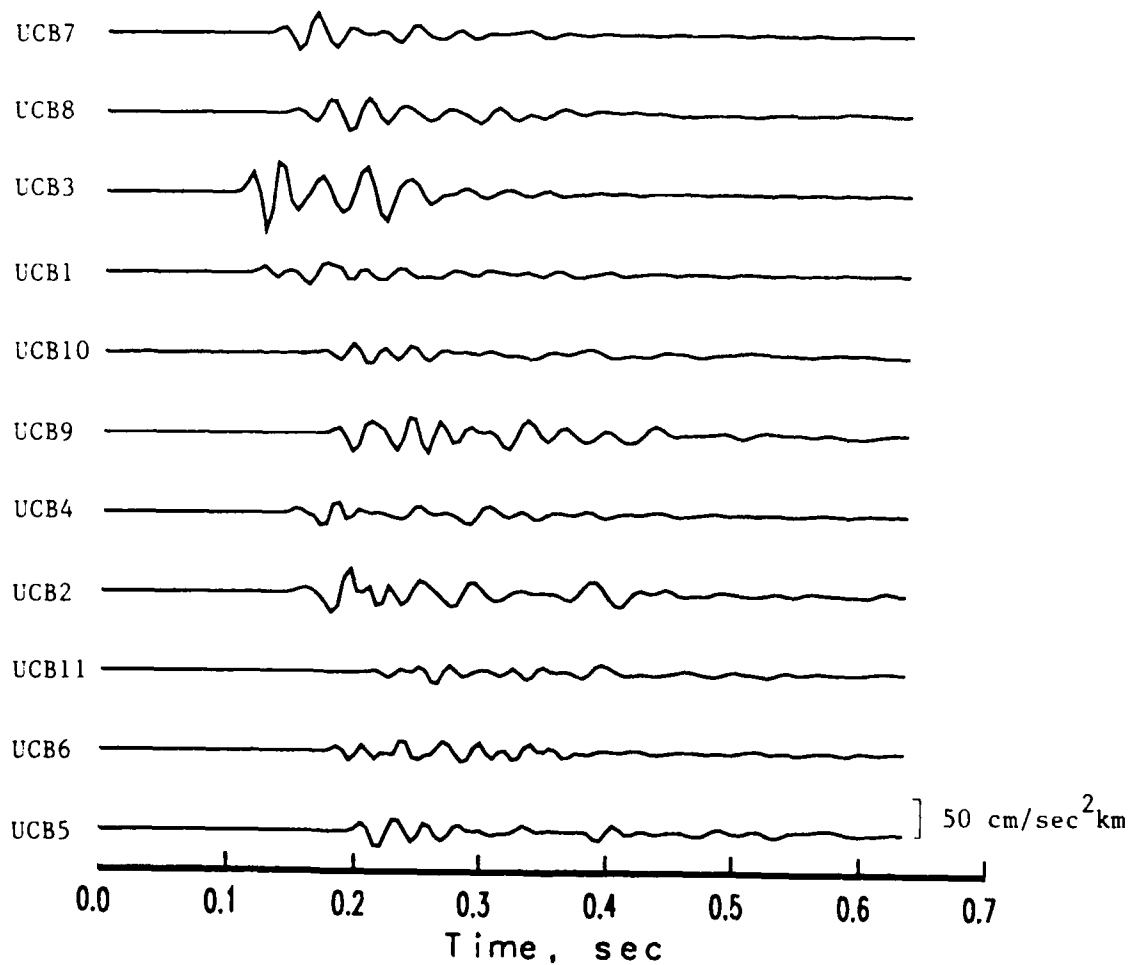


Figure 2. Radial accelerations of ground motion for event KQ1 which was a 1000 pound explosion at a depth of 217 meters. The label on the left indicates the recording station. The accelerations in this plot have been scaled by multiplying by the epicentral distance, but the maximum radial accelerations from this event were 0.20 g.

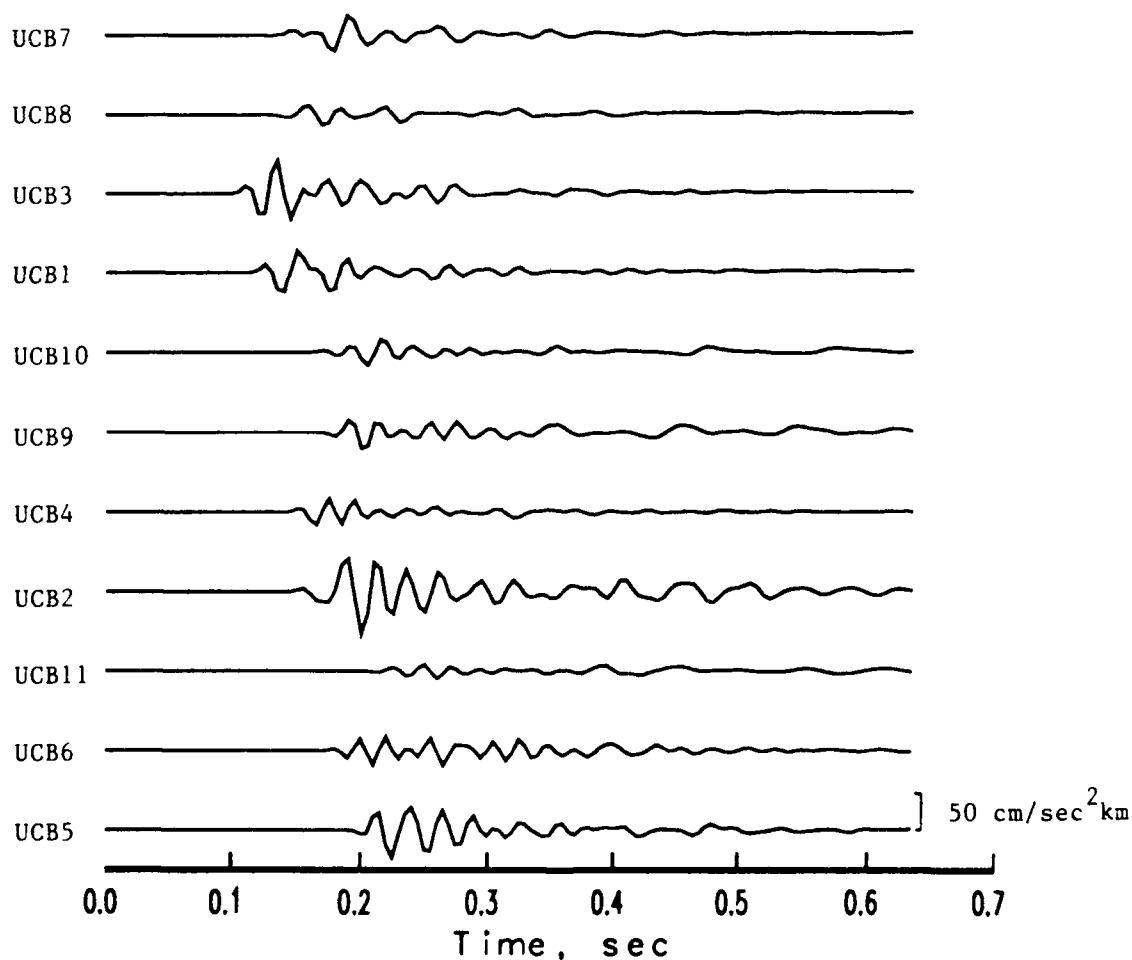


Figure 3. Transverse accelerations of ground motion for event KQ1 which was a 1000 pound explosion at a depth of 217 meters. The label on the left indicates the recording station. The accelerations in this plot have been scaled by multiplying by the epicentral distance, but the maximum transverse accelerations from this event were 0.17 g.

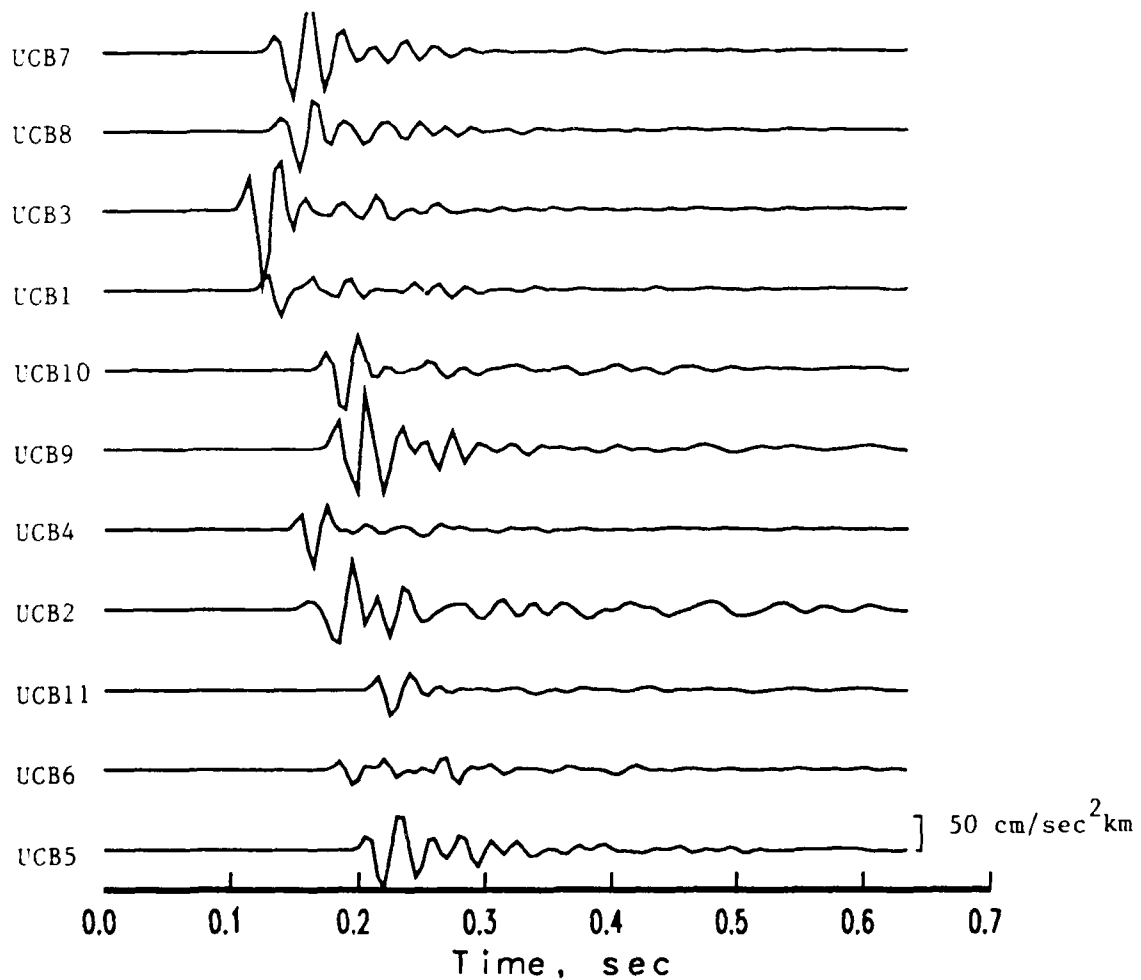


Figure 4. Vertical accelerations of ground motion for event KQ1 which was a 1000 pound explosion at a depth of 217 meters. The label on the left indicates the recording station. The accelerations in this plot have been scaled by multiplying by the epicentral distance, but the maximum vertical accelerations from this event were 0.40 g.

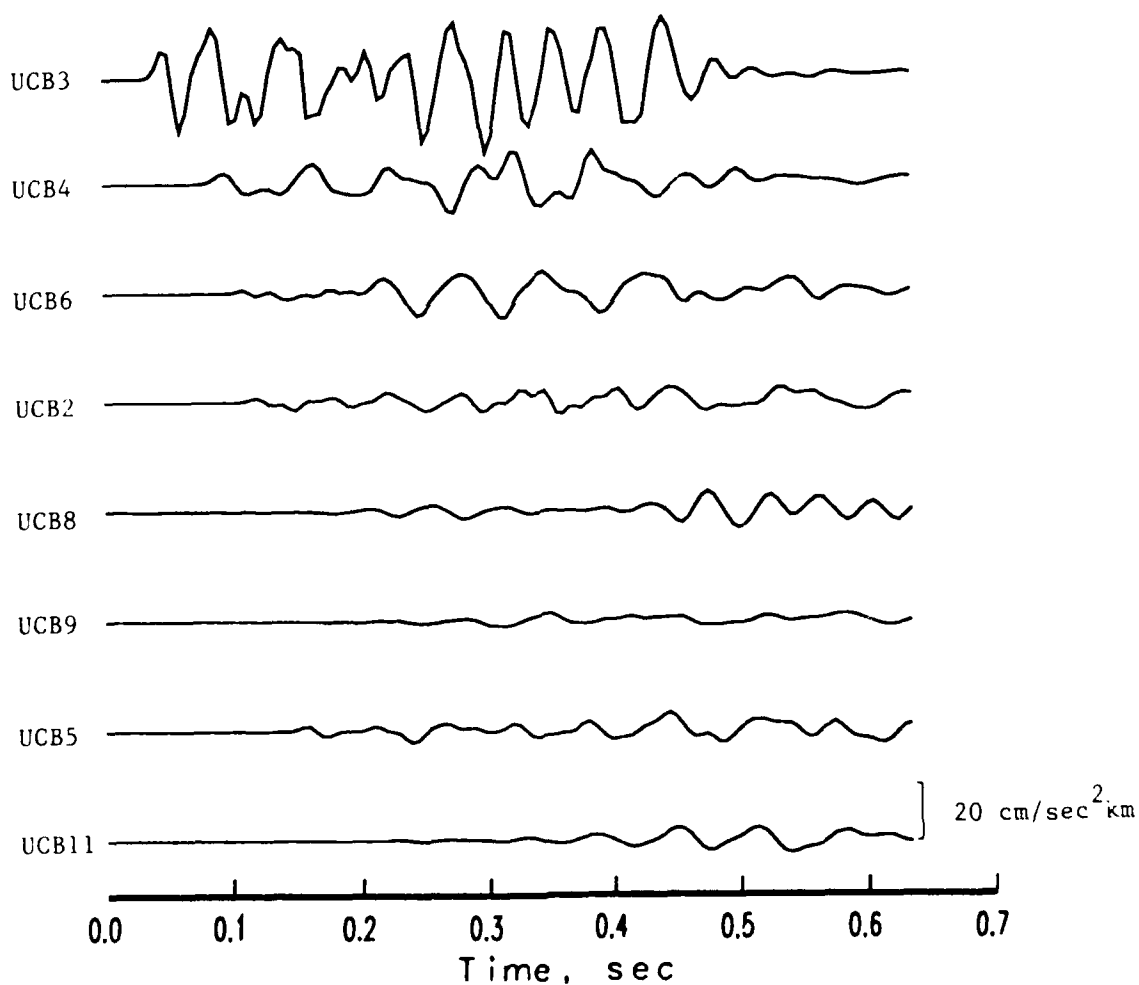


Figure 5. Radial accelerations of ground motion for event KQ2 which was a 7000 pound quarry blast distributed in 14 holes at a depth of 10 meters. The label on the left indicates the recording station. The accelerations in this plot have been scaled by multiplying by the epicentral distance, but the maximum radial accelerations from this event were 0.41 g.

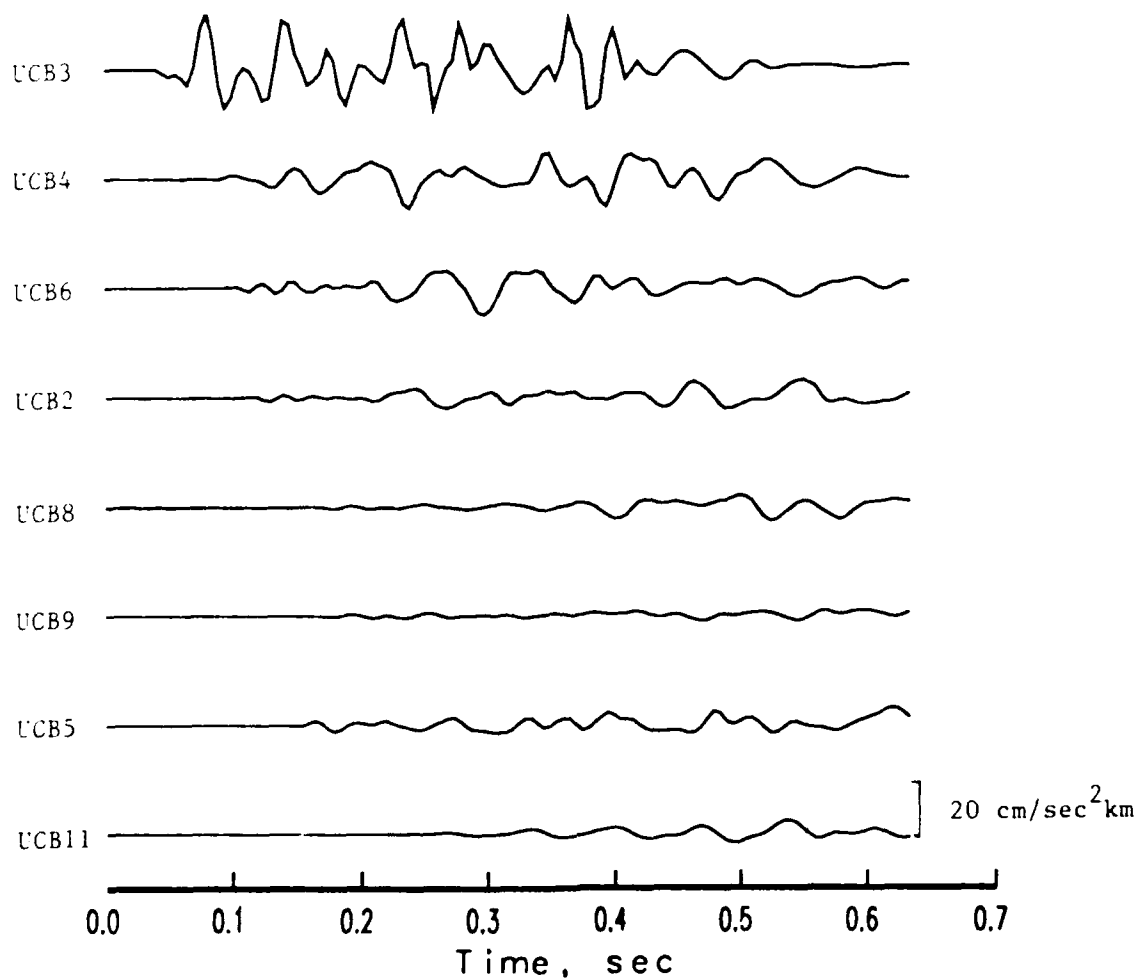


Figure 6. Transverse accelerations of ground motion for event KQ2 which was a 7000 pound quarry blast distributed in 14 holes at a depth of 10 meters. The label on the left indicates the recording station. The accelerations in this plot have been scaled by multiplying by the epicentral distance, but the maximum transverse accelerations from this event were 0.29 g.

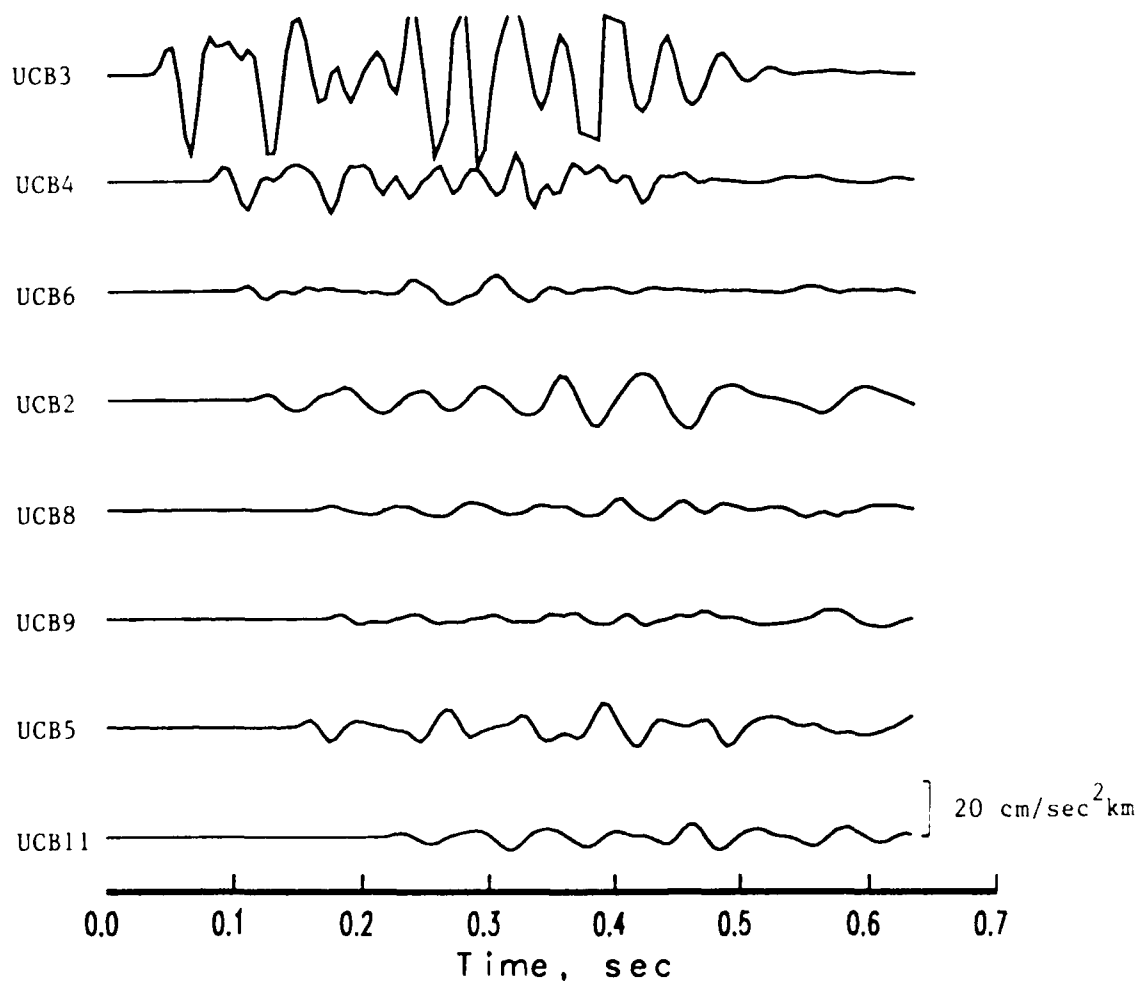


Figure 7. Vertical accelerations of ground motion for event KQ2 which was a 7000 pound quarry blast distributed in 14 holes at a depth of 10 meters. The label on the left indicates the recording station. The accelerations in this plot have been scaled by multiplying by the epicentral distance, but the maximum vertical accelerations from this event were 0.49 g.

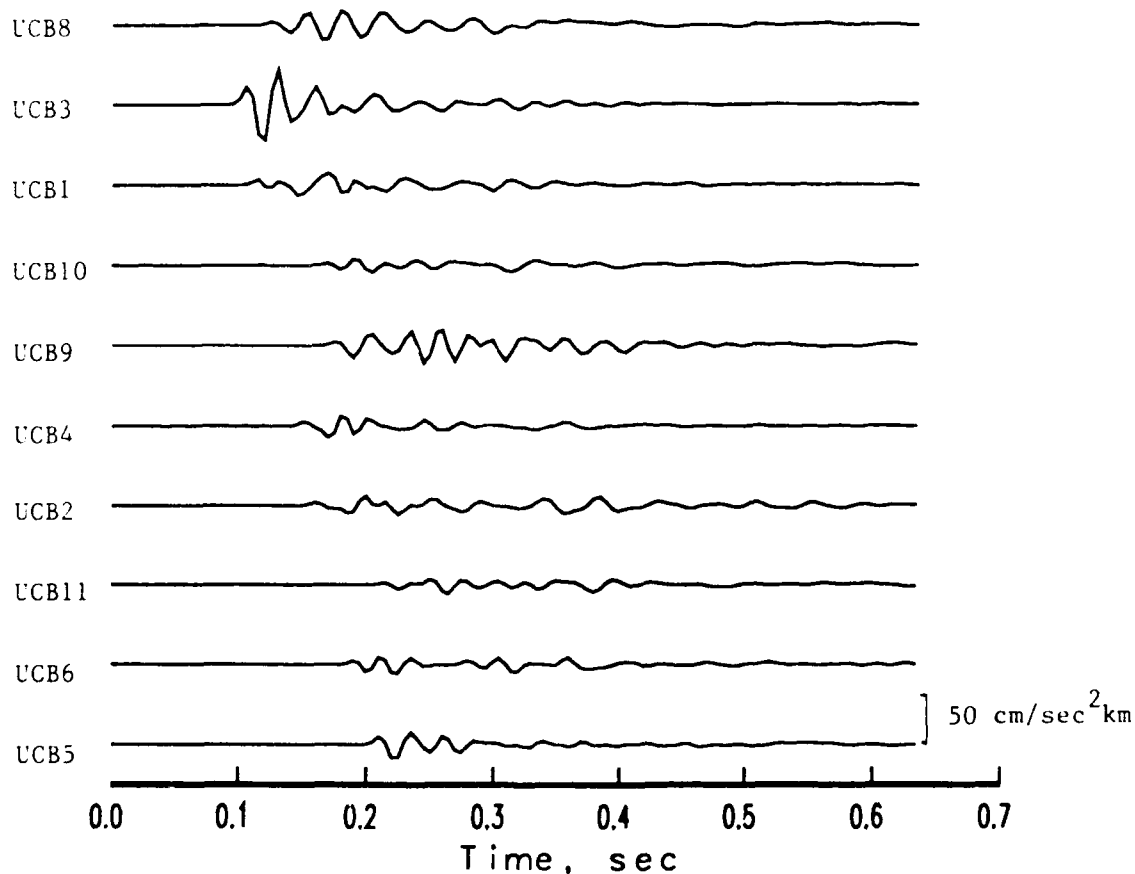


Figure 8. Radial accelerations of ground motion for event KQ3 which was a 900 pound explosion at a depth of 106 meters. The label on the left indicates the recording station. The accelerations in this plot have been scaled by multiplying by the epicentral distance, but the maximum radial accelerations from this event were 0.19 g.

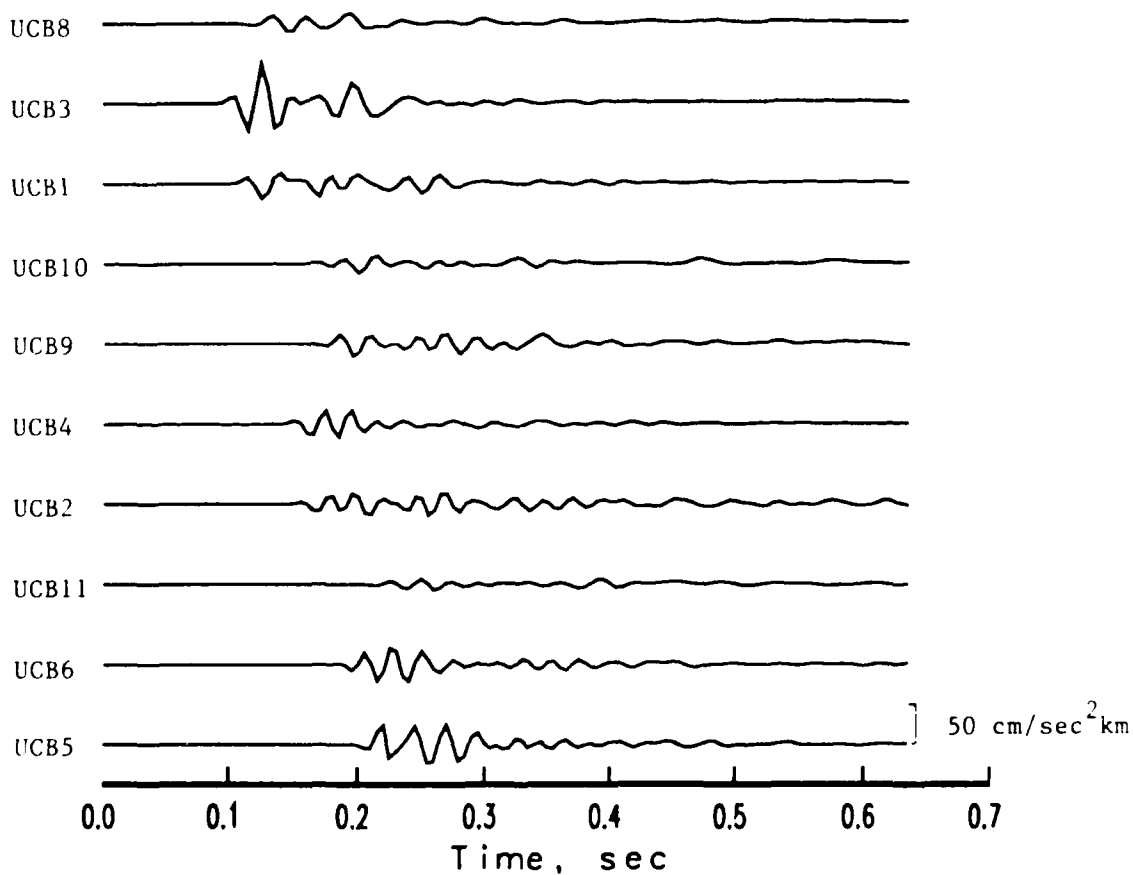


Figure 9. Transverse accelerations of ground motion for event KQ3 which was a 900 pound explosion at a depth of 106 meters. The label on the left indicates the recording station. The accelerations in this plot have been scaled by multiplying by the epicentral distance, but the maximum transverse accelerations from this event were 0.20 g.

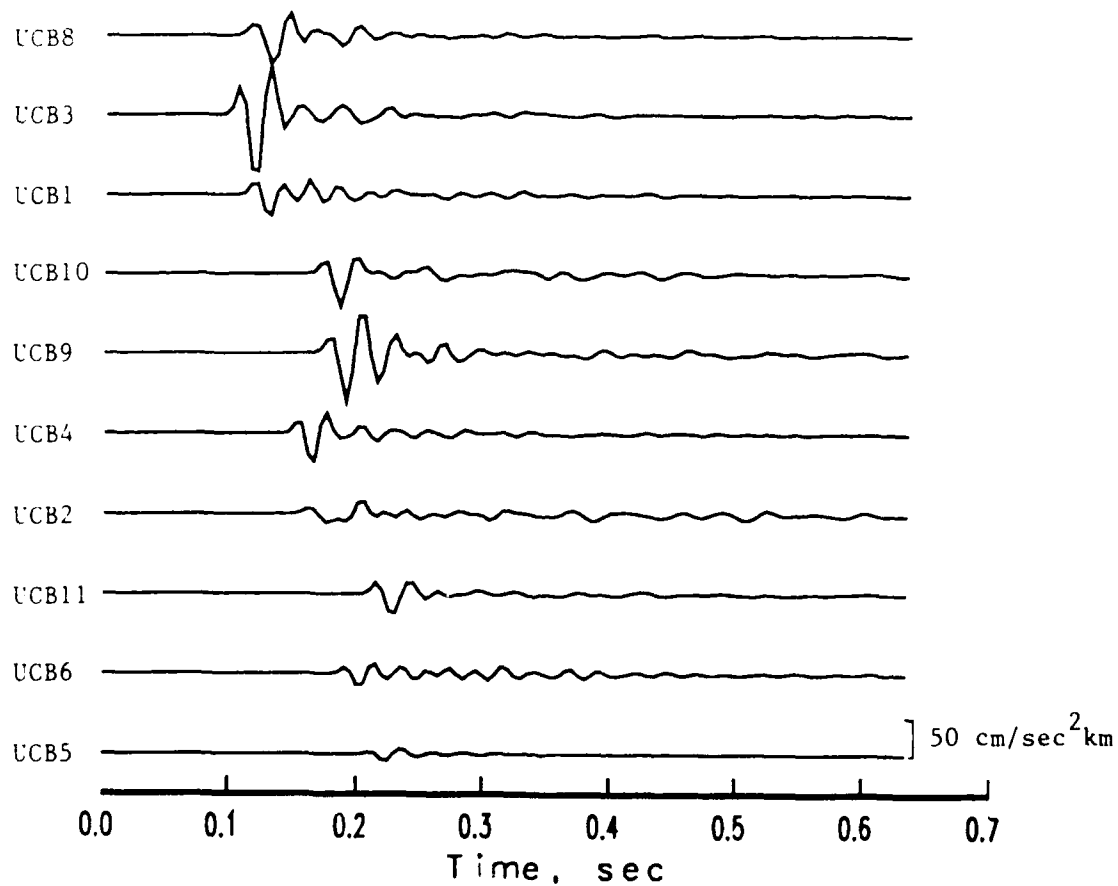


Figure 10. Vertical accelerations of ground motion for event KQ3 which was a 900 pound explosion at a depth of 106 meters. The label on the left indicates the recording station. The accelerations in this plot have been scaled by multiplying by the epicentral distance, but the maximum vertical accelerations from this event were 0.30 g.

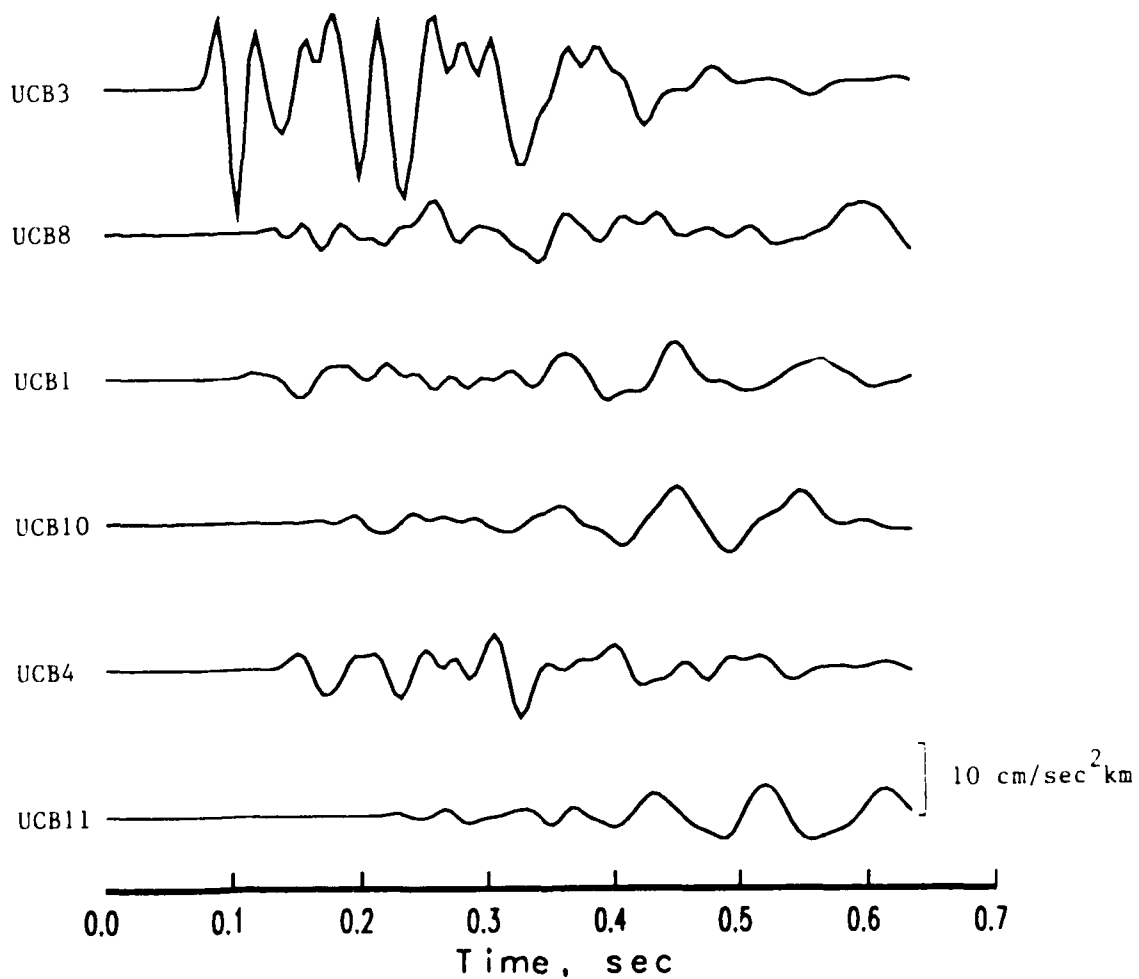


Figure 11. Radial accelerations of ground motion for event KQ4 which was a 1900 pound quarry blast distributed over 4 holes at a depth of 10 meters. The label on the left indicates the recording station. The accelerations in this plot have been scaled by multiplying by the epicentral distance, but the maximum radial accelerations from this event were 0.10 g.

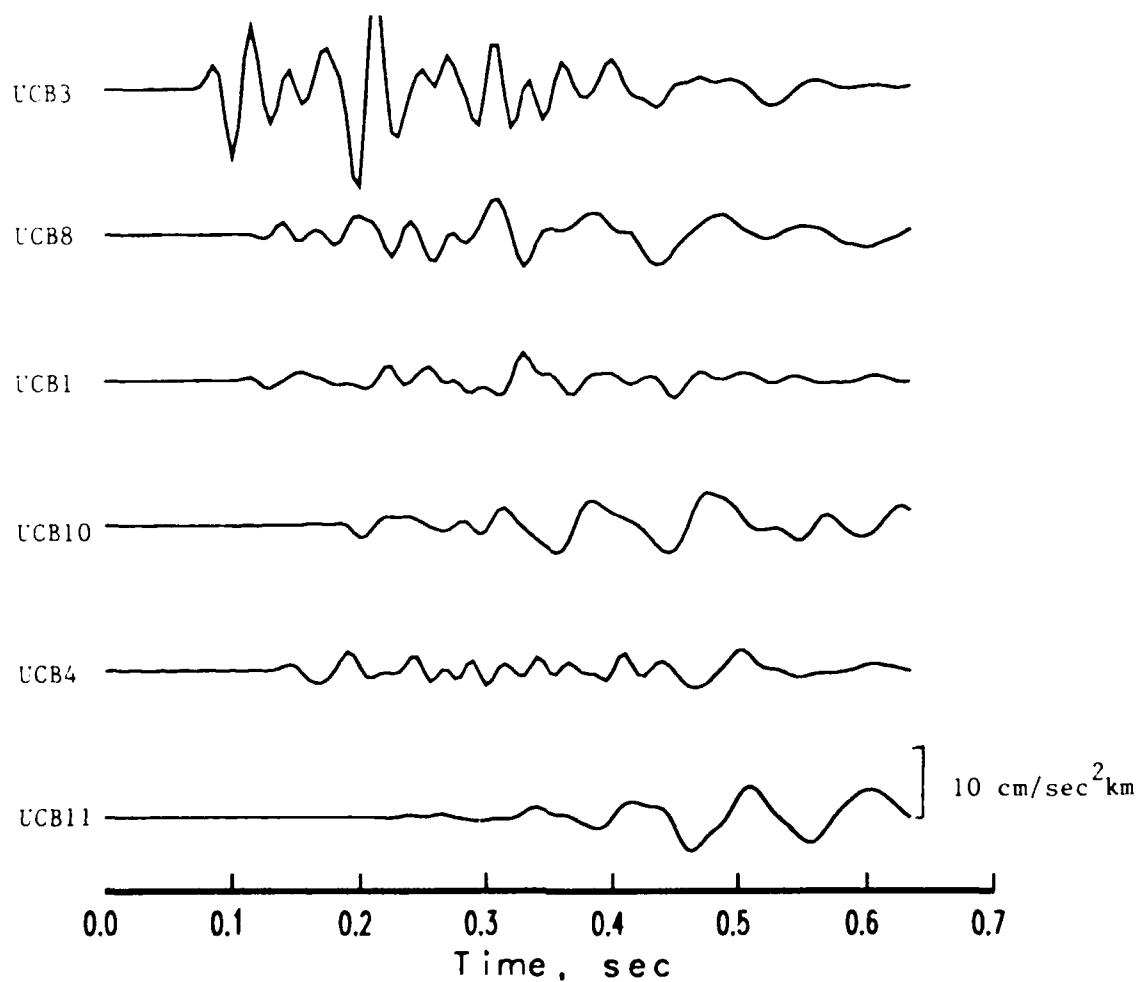


Figure 12. Transverse accelerations of ground motion for event KQ4 which was a 1900 pound quarry blast distributed over 4 holes at a depth of 10 meters. The label on the left indicates the recording station. The accelerations in this plot have been scaled by multiplying by the epicentral distance, but the maximum transverse accelerations from this event were 0.08 g.

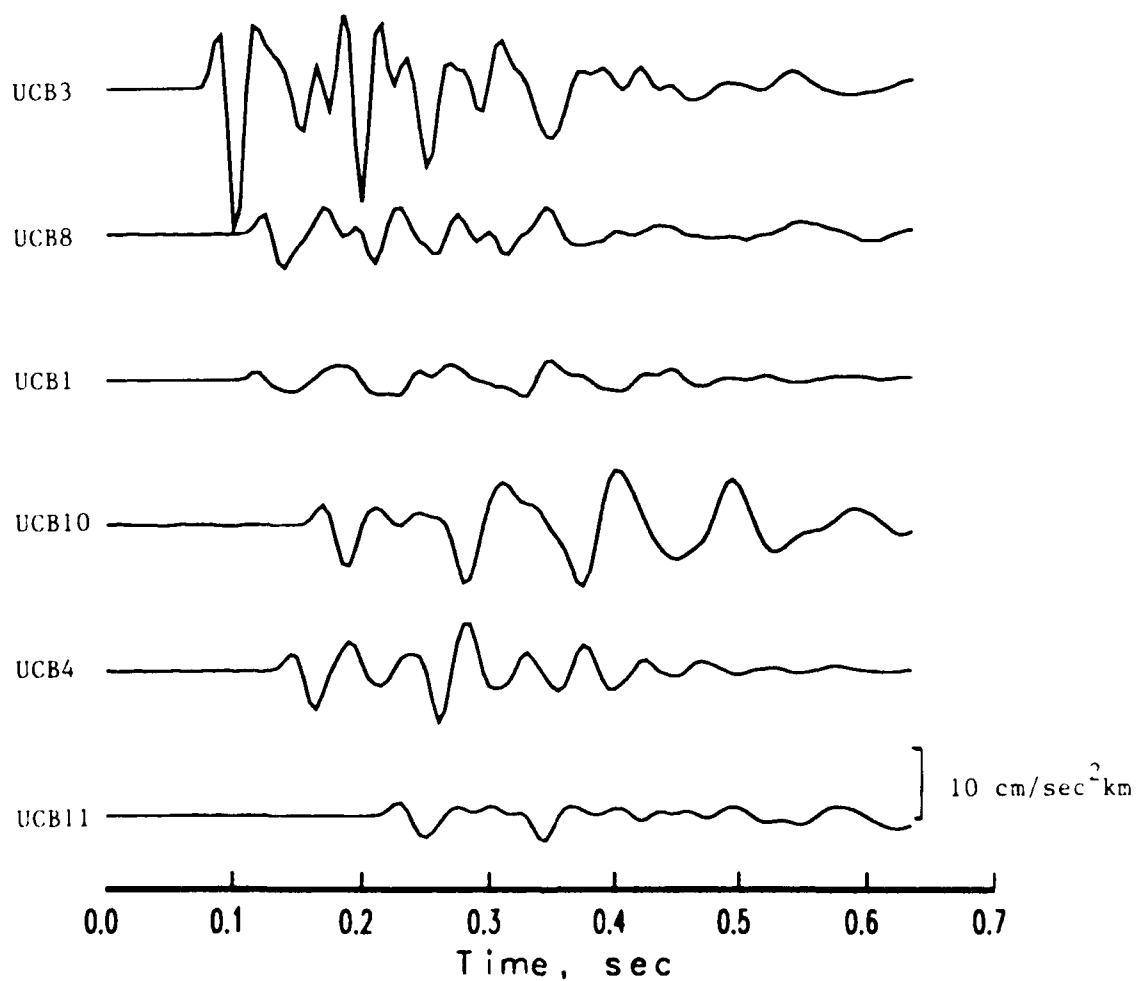


Figure 13. Vertical accelerations of ground motion for event KQ4 which was a 1900 pound quarry blast distributed over 4 holes at a depth of 10 meters. The label on the left indicates the recording station. The accelerations in this plot have been scaled by multiplying by the epicentral distance, but the maximum vertical accelerations from this event were 0.11 g.

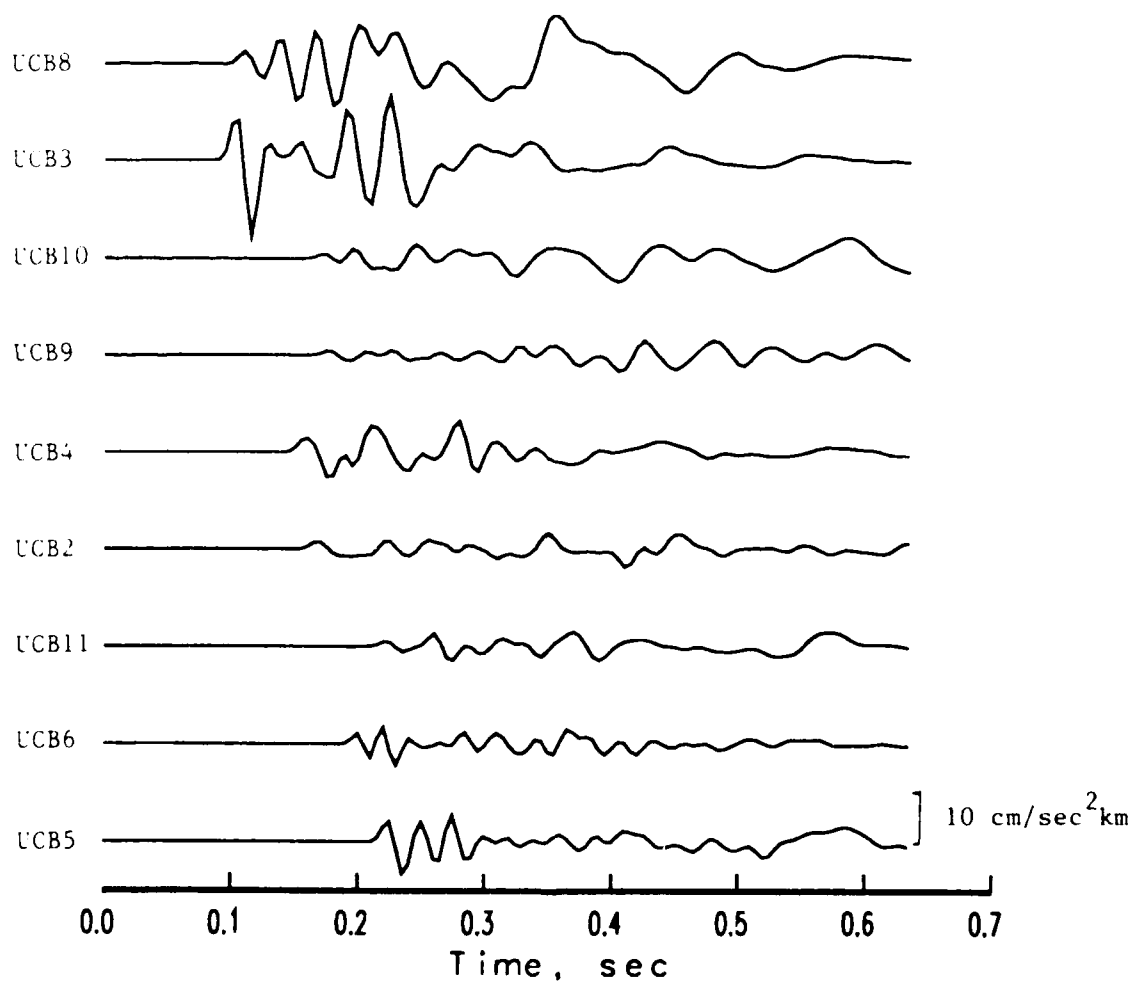


Figure 14. Radial accelerations of ground motion for event KQ5 which was a 900 pound explosion at a depth of 42 meters. The label on the left indicates the recording station. The accelerations in this plot have been scaled by multiplying by the epicentral distance, but the maximum radial accelerations from this event were 0.07 g.

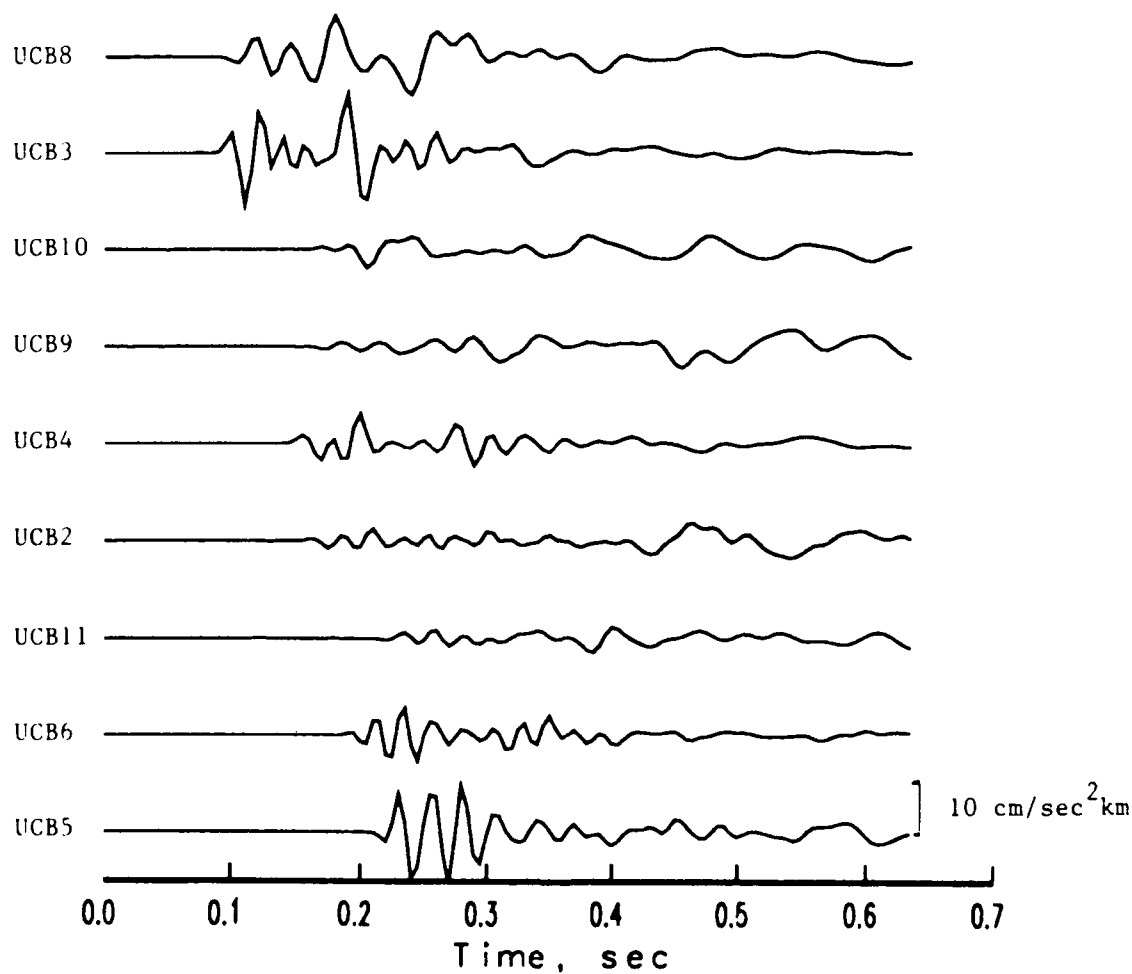


Figure 15. Transverse accelerations of ground motion for event KQ5 which was a 900 pound explosion at a depth of 42 meters. The label on the left indicates the recording station. The accelerations in this plot have been scaled by multiplying by the epicentral distance, but the maximum transverse accelerations from this event were 0.05 g.

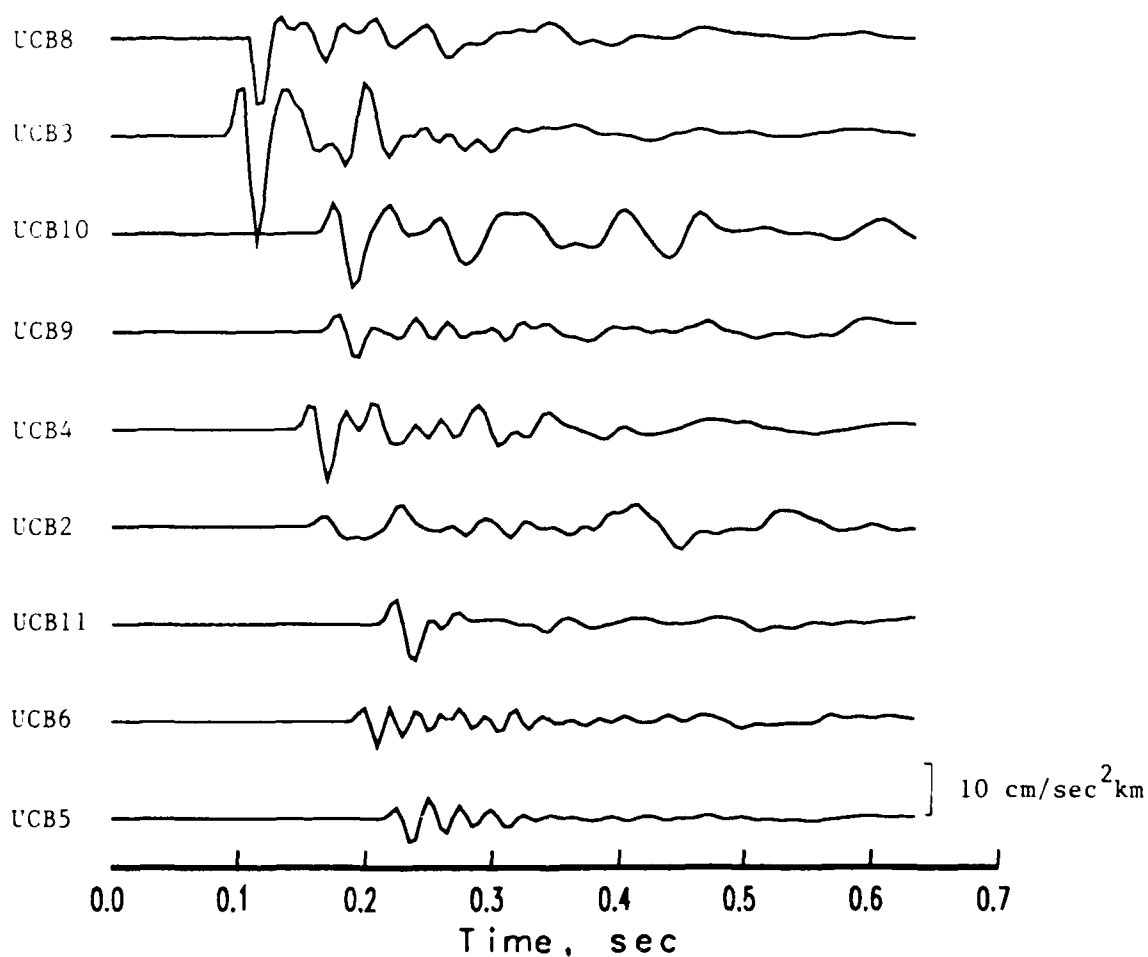


Figure 16. Vertical accelerations of ground motion for event KQ5 which was a 900 pound explosion at a depth of 42 meters. The label on the left indicates the recording station. The accelerations in this plot have been scaled by multiplying by the epicentral distance, but the maximum vertical accelerations from this event were 0.09 g.

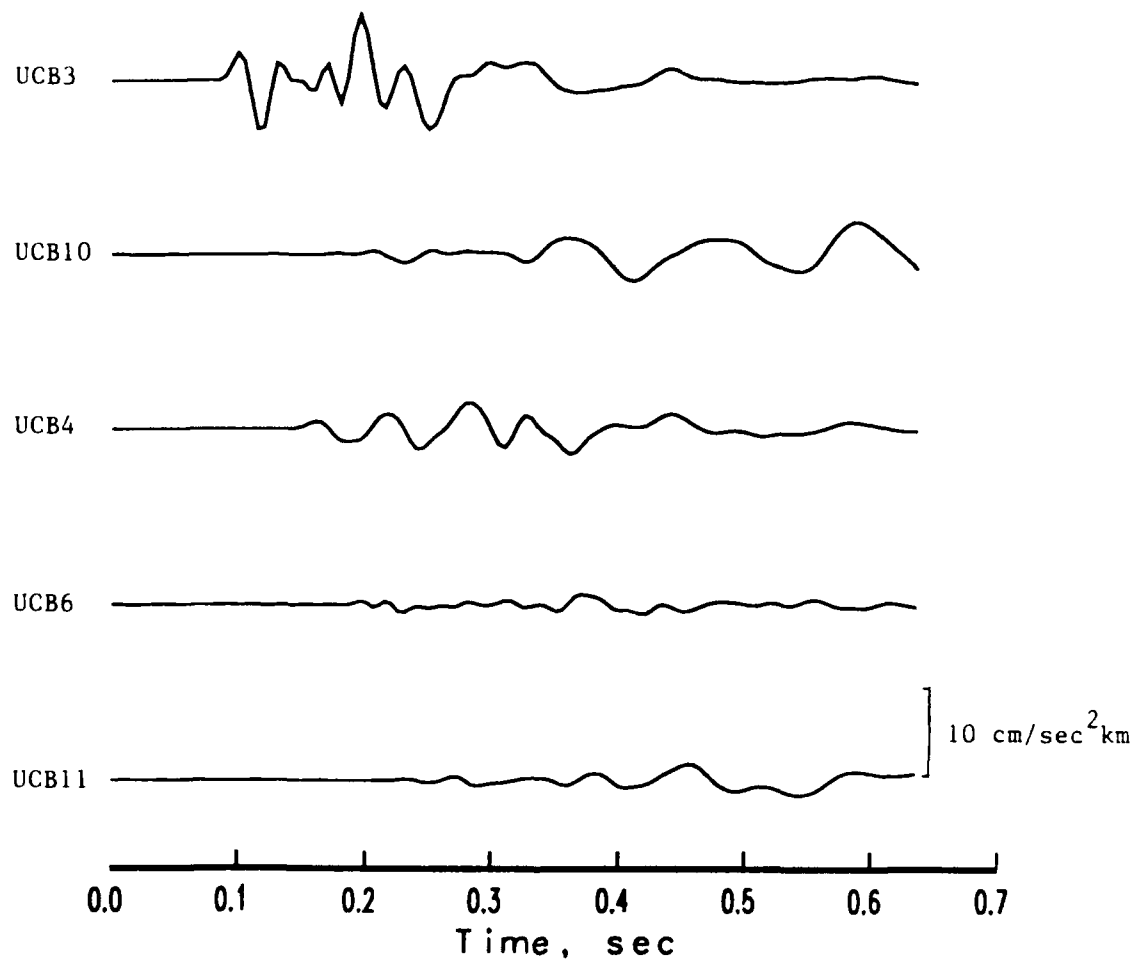


Figure 17. Radial accelerations of ground motion for event KQ8 which was a 340 pound explosion at a depth of 10 meters. The label on the left indicates the recording station. The accelerations in this plot have been scaled by multiplying by the epicentral distance, but the maximum radial accelerations from this event were 0.04 g.

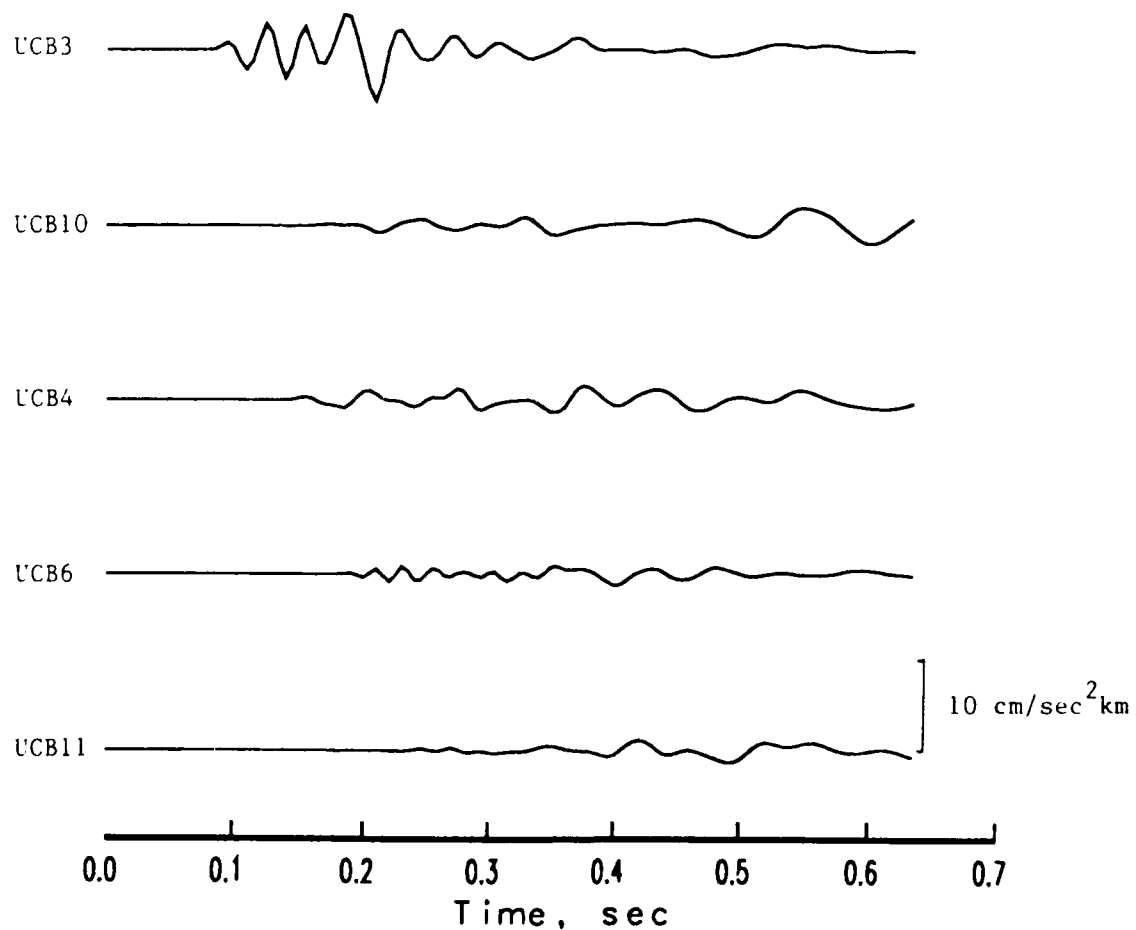


Figure 18. Transverse accelerations of ground motion for event KQ8 which was a 340 pound explosion at a depth of 10 meters. The label on the left indicates the recording station. The accelerations in this plot have been scaled by multiplying by the epicentral distance, but the maximum transverse accelerations from this event were 0.03 g.

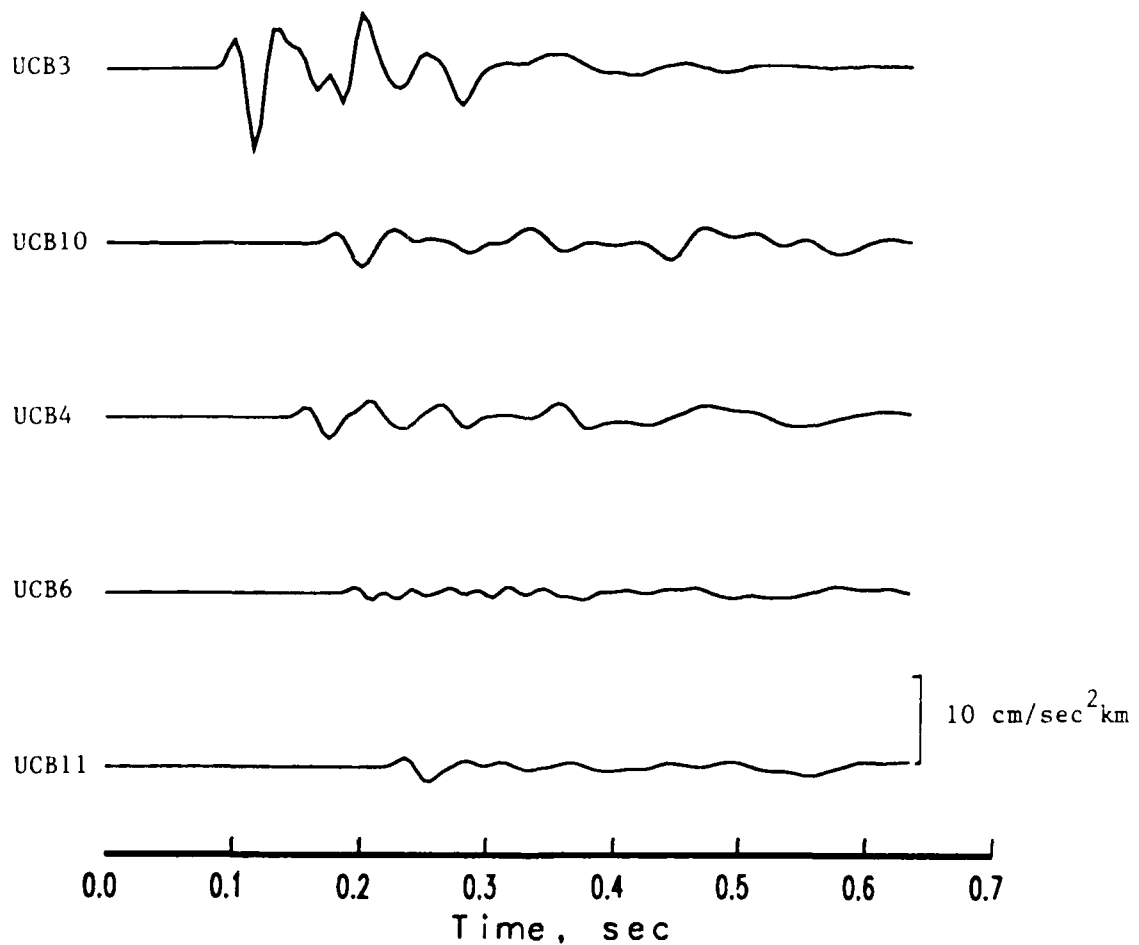


Figure 19. Vertical accelerations of ground motion for event KQ8 which was a 340 pound explosion at a depth of 10 meters. The label on the left indicates the recording station. The accelerations in this plot have been scaled by multiplying by the epicentral distance, but the maximum vertical accelerations from this event were 0.04 g.

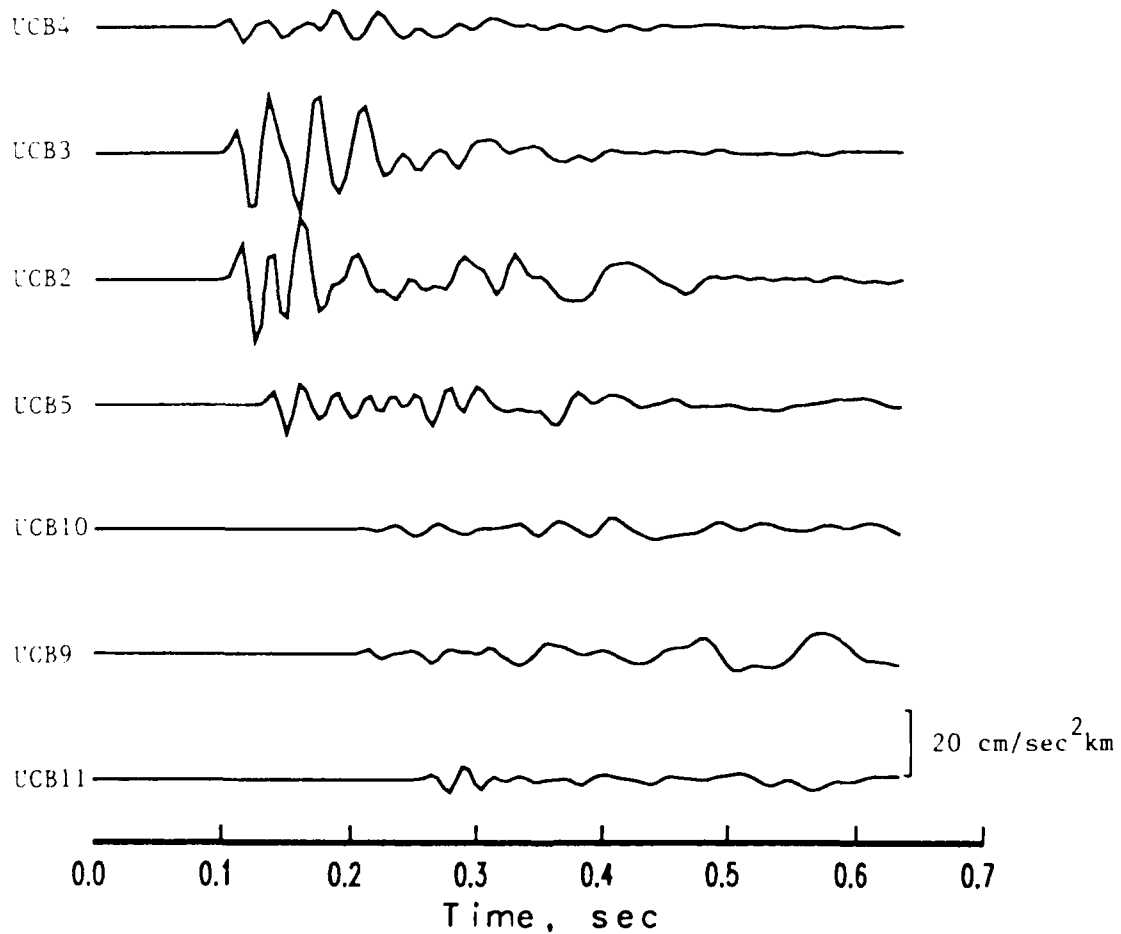


Figure 20. Radial accelerations of ground motion for event KQ9 which was a 300 pound explosion at a depth of 12 meters. The label on the left indicates the recording station. The accelerations in this plot have been scaled by multiplying by the epicentral distance, but the maximum radial accelerations from this event were 0.07 g.

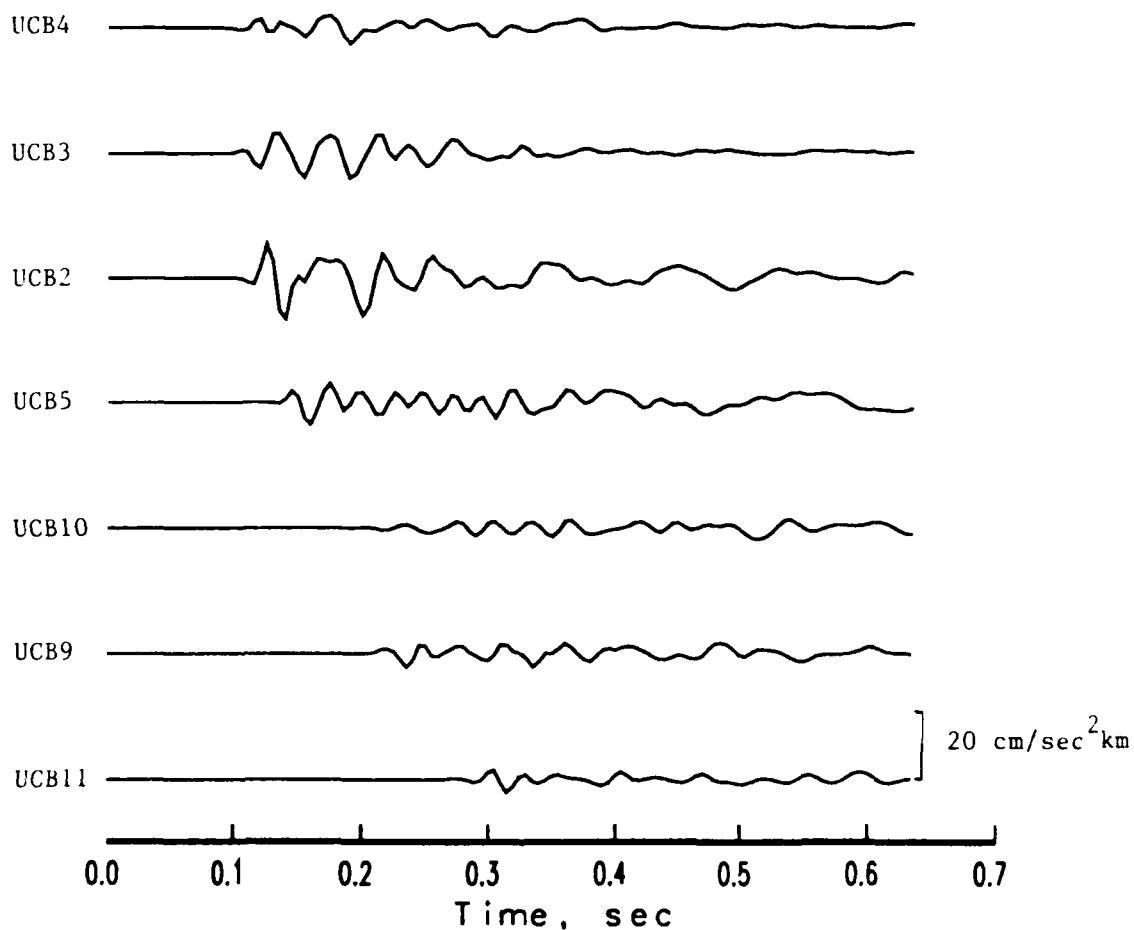


Figure 21. Transverse accelerations of ground motion for event KQ9 which was a 300 pound explosion at a depth of 12 meters. The label on the left indicates the recording station. The accelerations in this plot have been scaled by multiplying by the epicentral distance, but the maximum transverse accelerations from this event were 0.05 g.

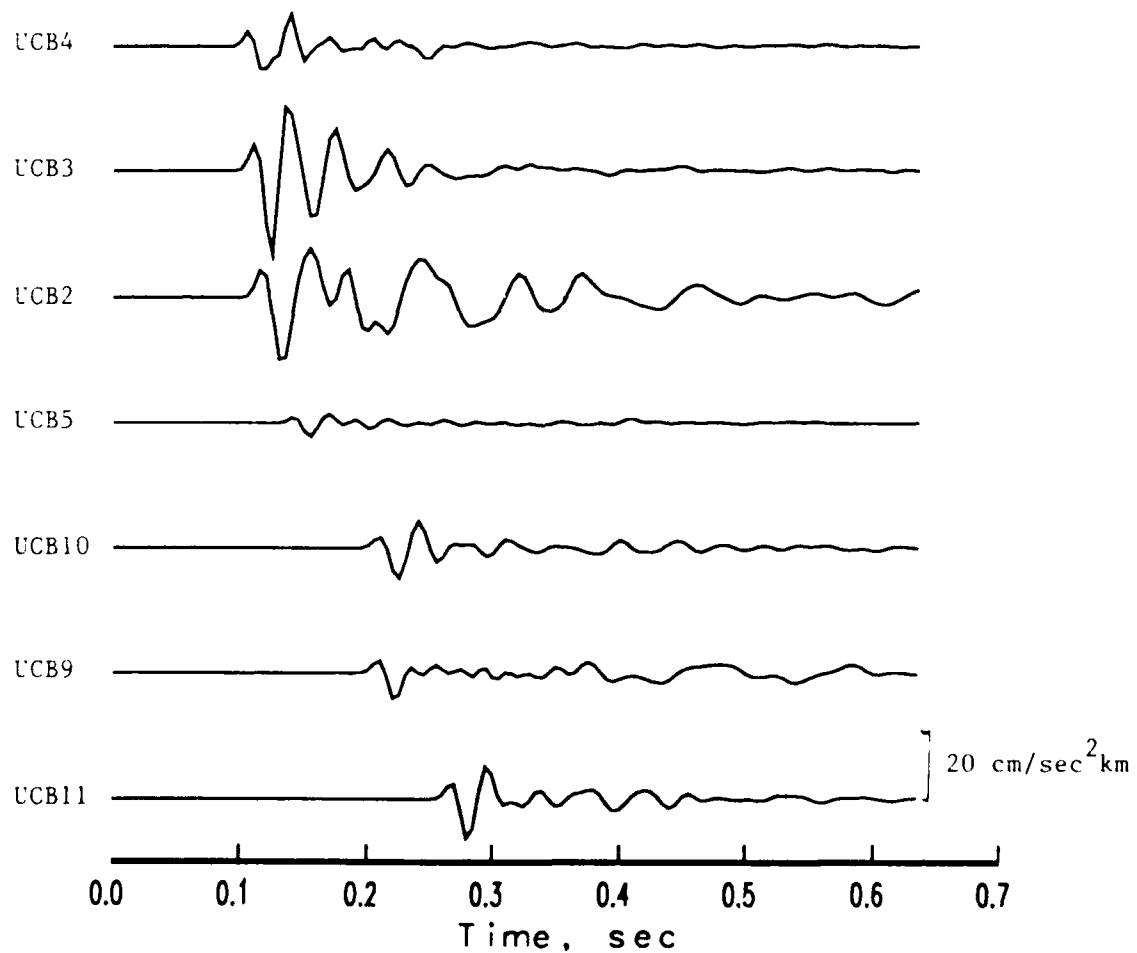


Figure 22. Vertical accelerations of ground motion for event KQ9 which was a 300 pound explosion at a depth of 12 meters. The label on the left indicates the recording station. The accelerations in this plot have been scaled by multiplying by the epicentral distance, but the maximum vertical accelerations from this event were 0.10 g.

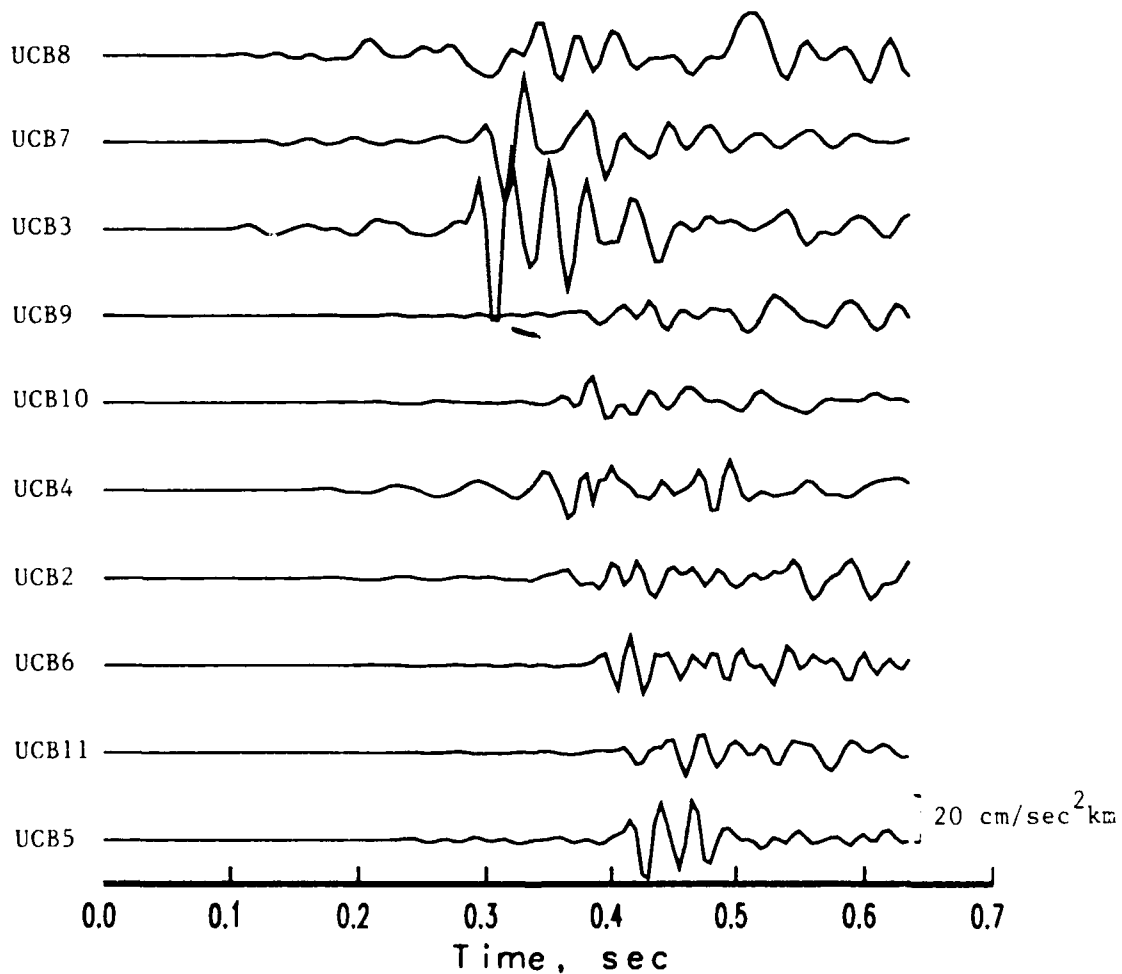


Figure 23. Radial accelerations of ground motion for event KQ10 which was a 11,900 pound quarry blast distributed over 23 holes at a depth of 10 meters followed 0.1 sec later by a 1,000 pound explosion at a depth of 81 meters. The label on the left indicates the recording station. The accelerations in this plot have been scaled by multiplying by the epicentral distance, but the maximum radial accelerations from this event were 0.17 g.

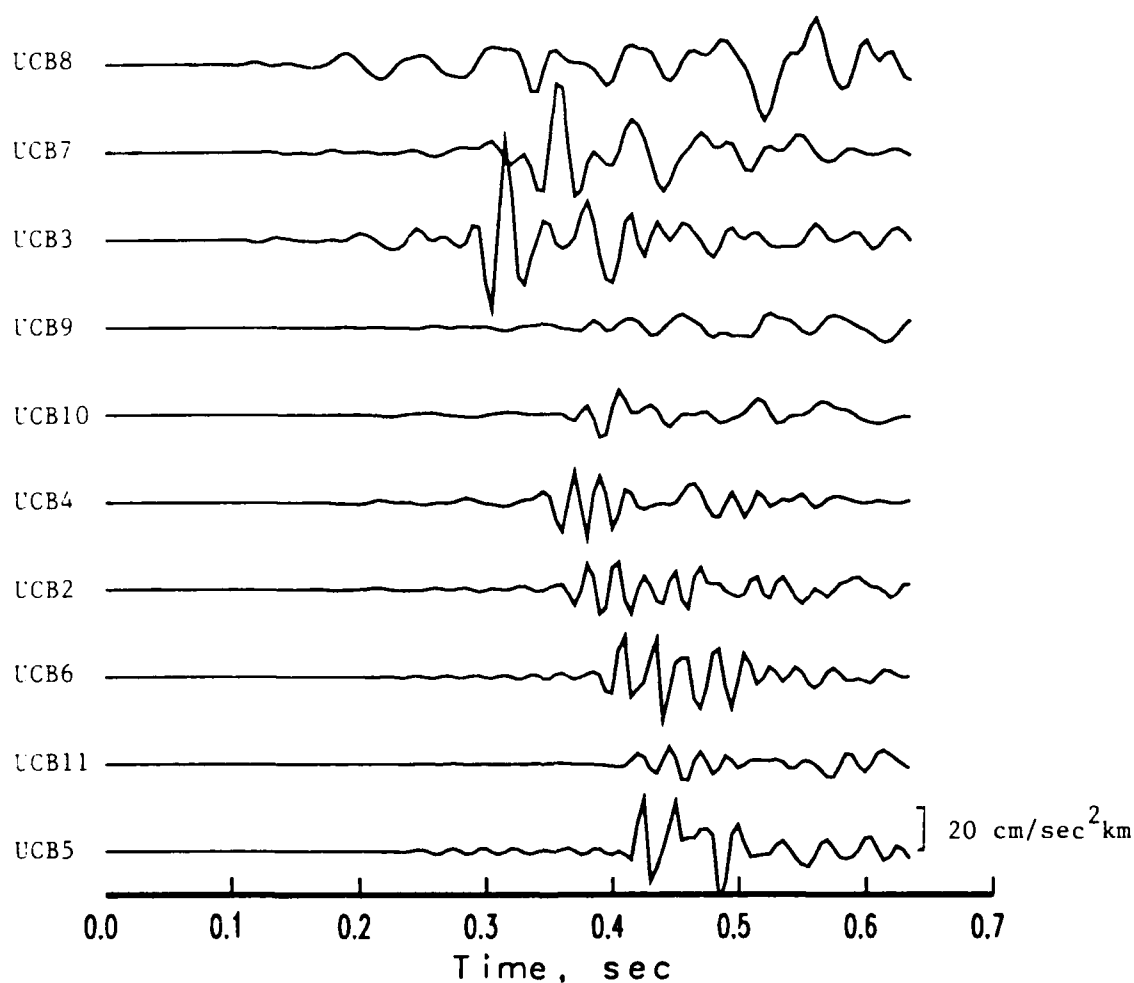


Figure 24. Transverse accelerations of ground motion for event KQ10 which was a 11,900 pound quarry blast distributed over 23 holes at a depth of 10 meters followed 0.1 sec later by a 1,000 pound explosion at a depth of 81 meters. The label on the left indicates the recording station. The accelerations in this plot have been scaled by multiplying by the epicentral distance, but the maximum transverse accelerations from this event were 0.19 g.

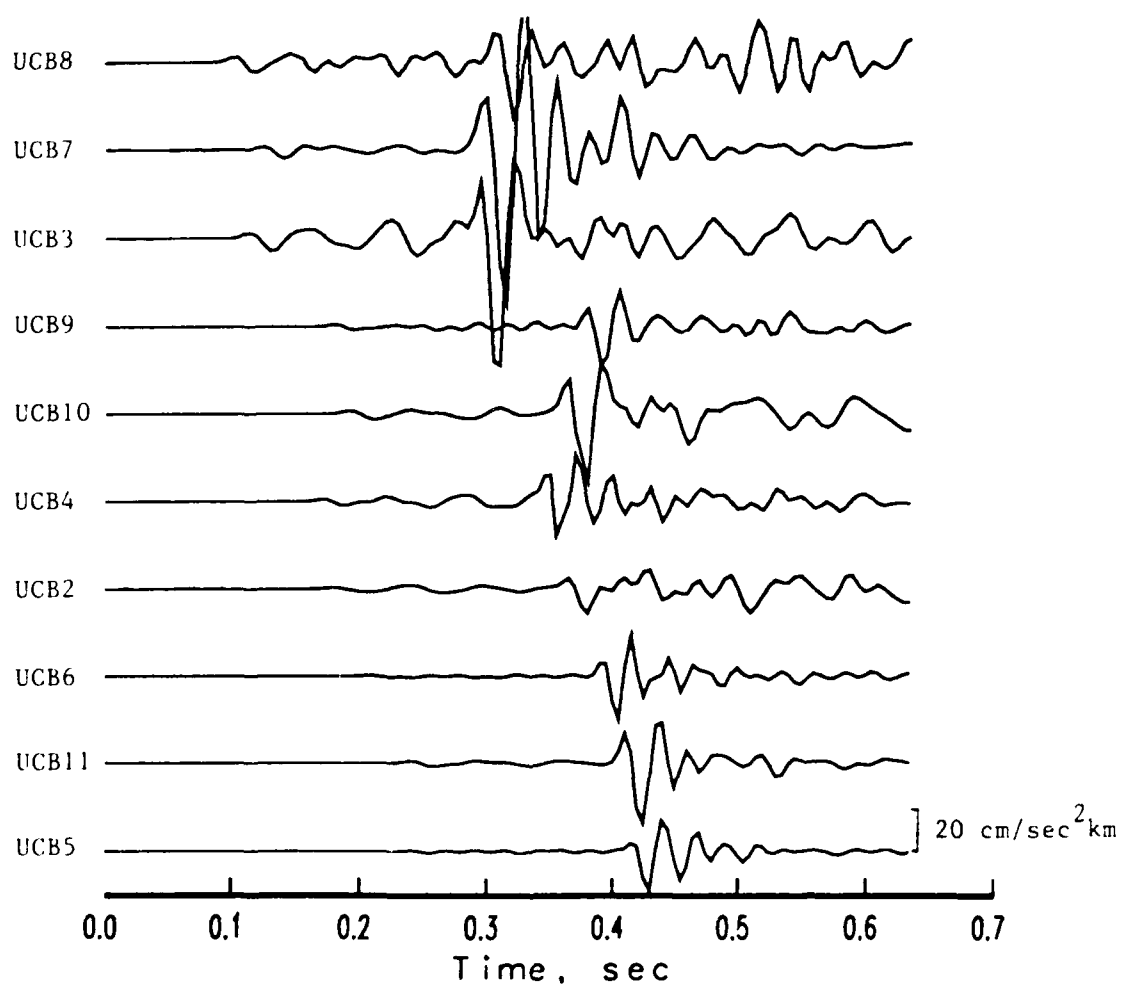


Figure 25. Vertical accelerations of ground motion for event KQ10 which was a 11,900 pound quarry blast distributed over 23 holes at a depth of 10 meters followed 0.1 sec later by a 1,000 pound explosion at a depth of 81 meters. The label on the left indicates the recording station. The accelerations in this plot have been scaled by multiplying by the epicentral distance, but the maximum vertical accelerations from this event were 0.35 g.

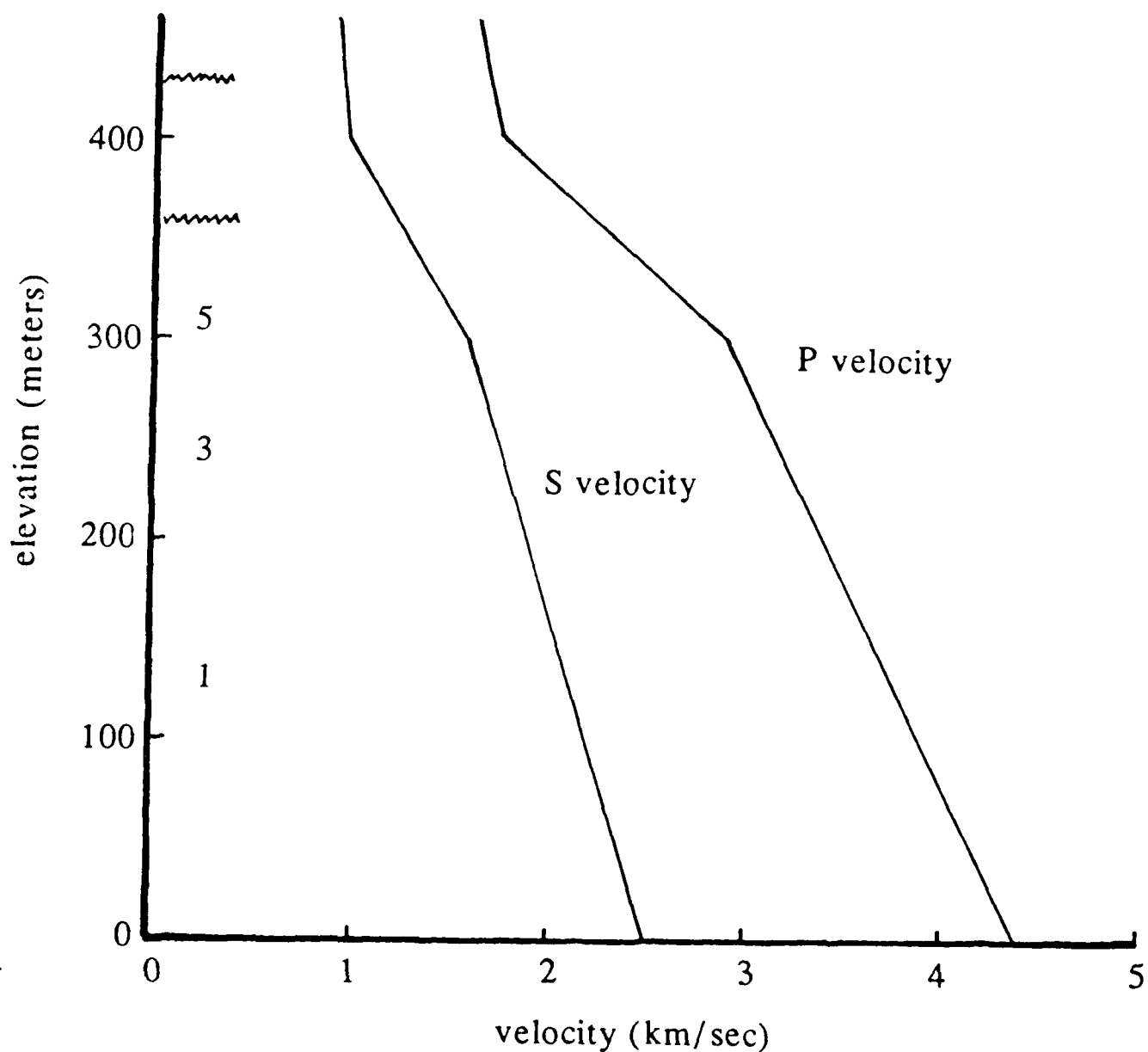


Figure 26. Estimates of the average P and S velocities as a function of elevation in the Kaiser Permanente Quarry. The boundaries at elevations of 360 and 430 meters indicate the approximate floor and rim, respectively, of the quarry. The numbers 1, 3, and 5 indicate the locations of the 3 explosions KQ01, KQ03 and KQ05 in the same drilled hole.

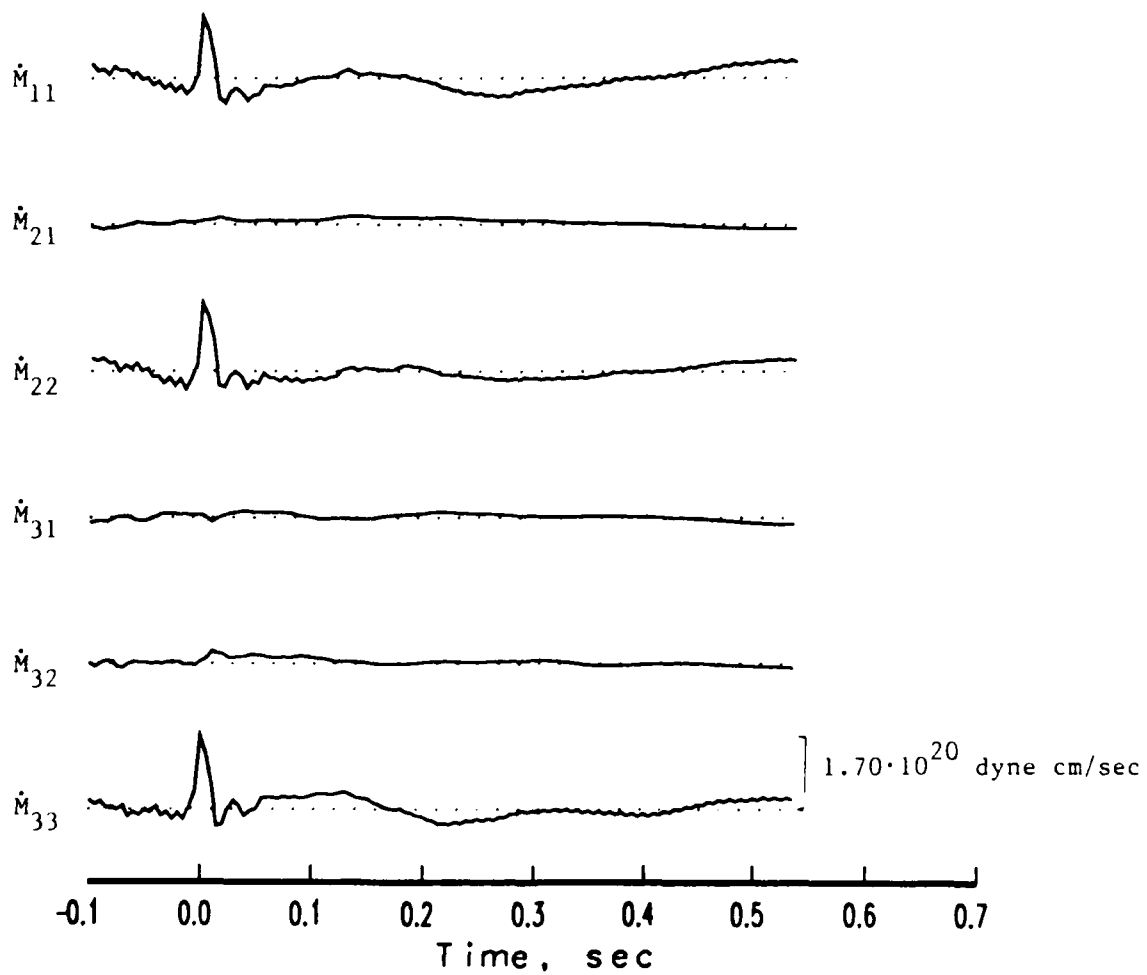


Figure 27. Second-order force-moment rate tensors which were estimated for the event KQ01.

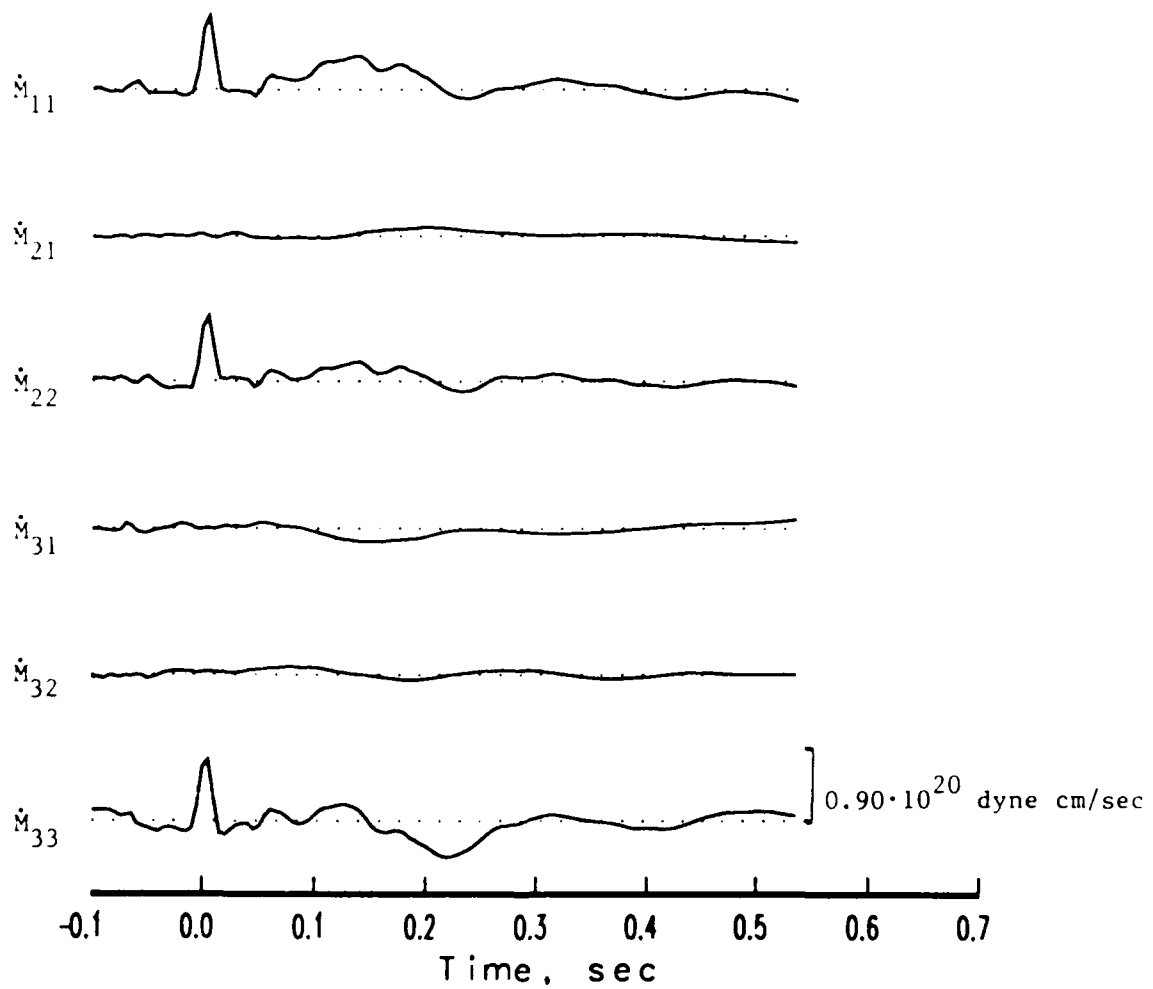


Figure 28. Second-order force-moment rate tensors which were estimated for the event KQ03.

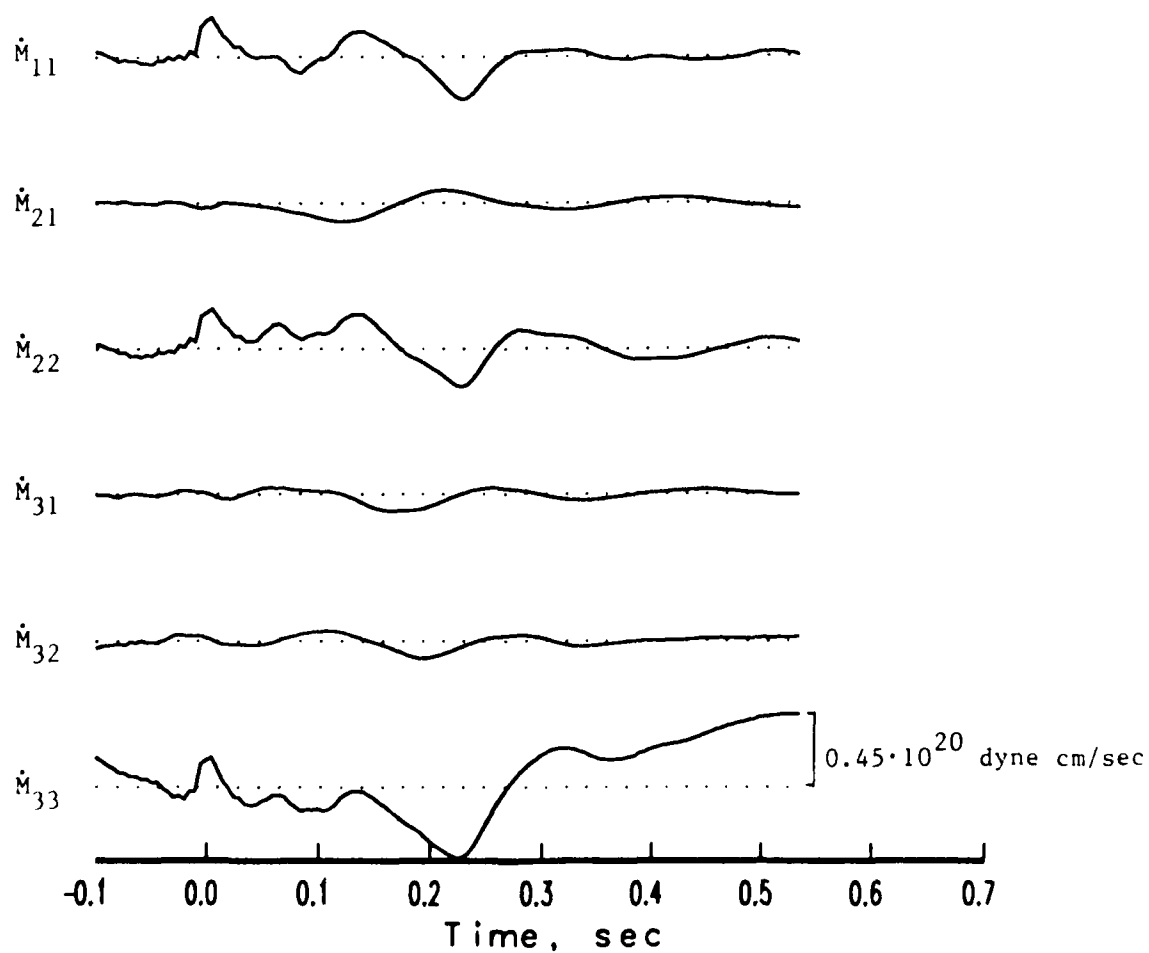


Figure 29. Second-order force-moment rate tensors which were estimated for the event KQ05.

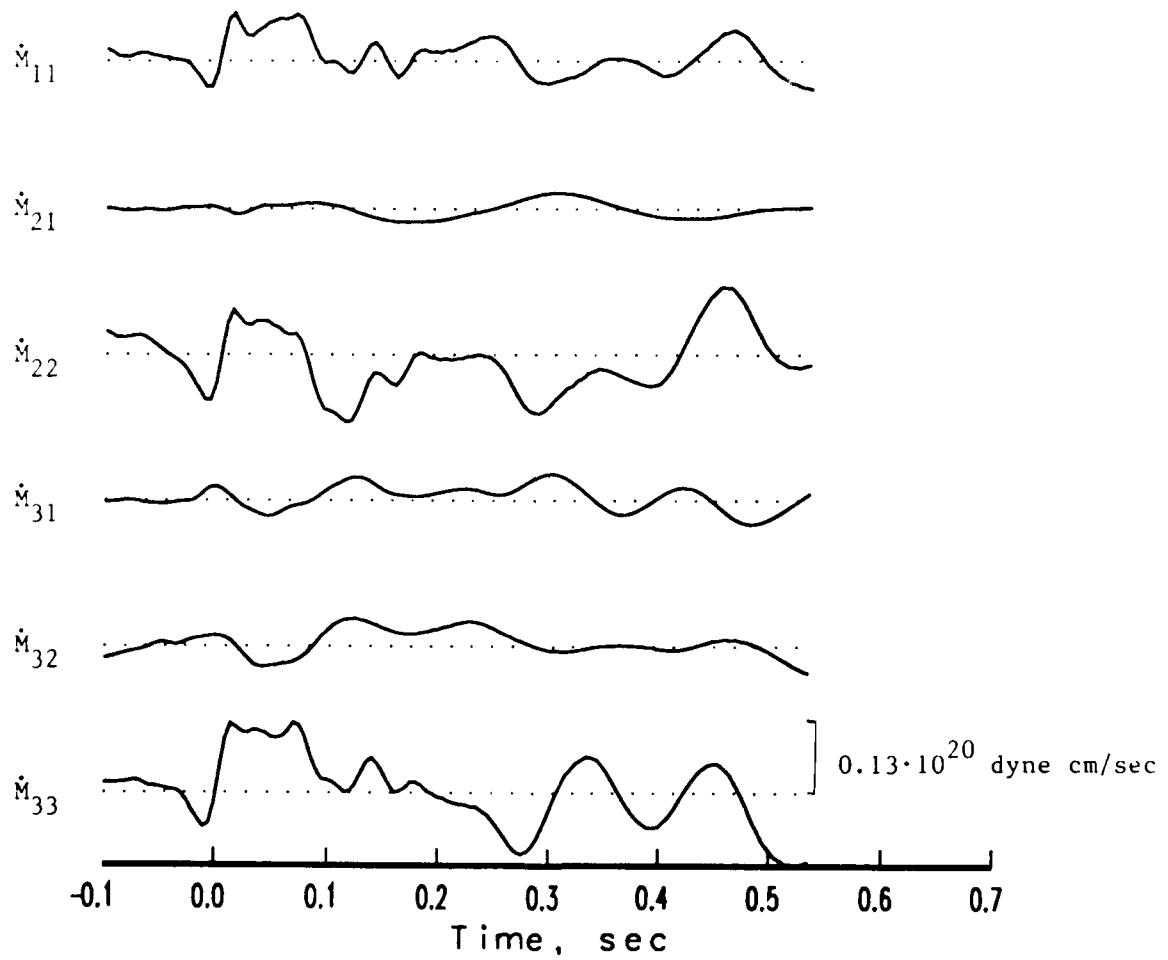


Figure 30. Second-order force-moment rate tensors which were estimated for the event KQ08.

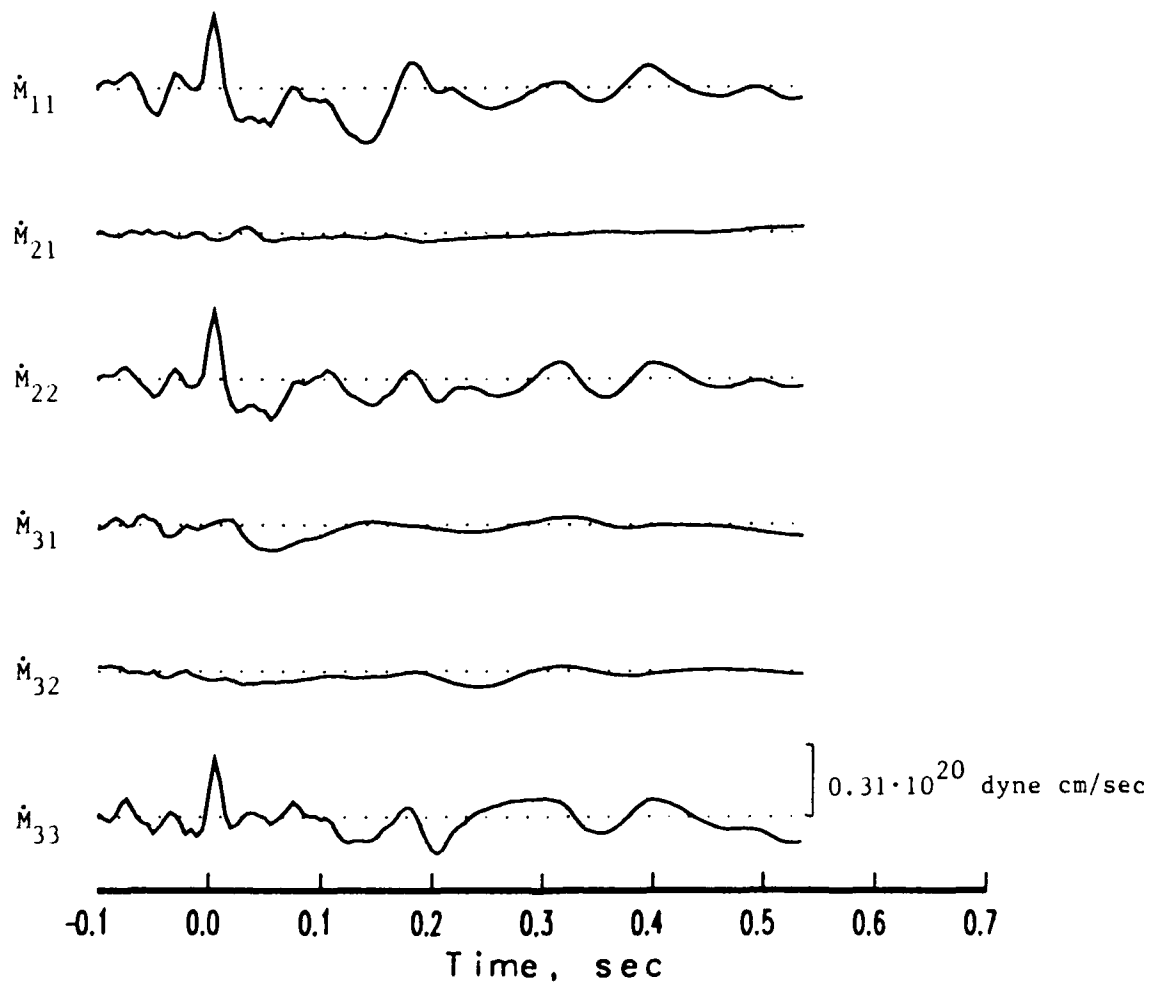


Figure 31. Second-order force-moment rate tensors which were estimated for the event KQ09.

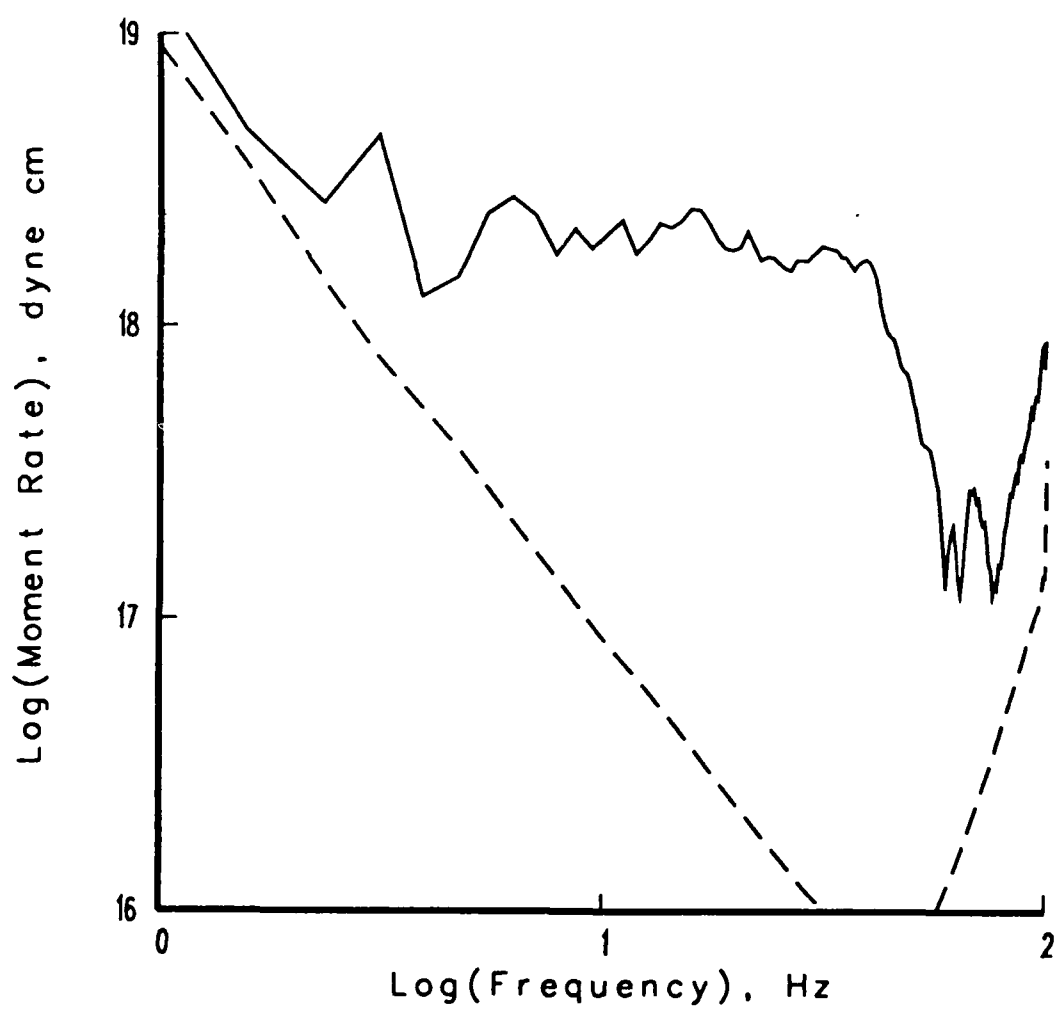


Figure 32. Amplitude density spectrum of the isotropic part of the moment rate tensor estimated for the event KQ01. The dashed line is the estimated standard error.

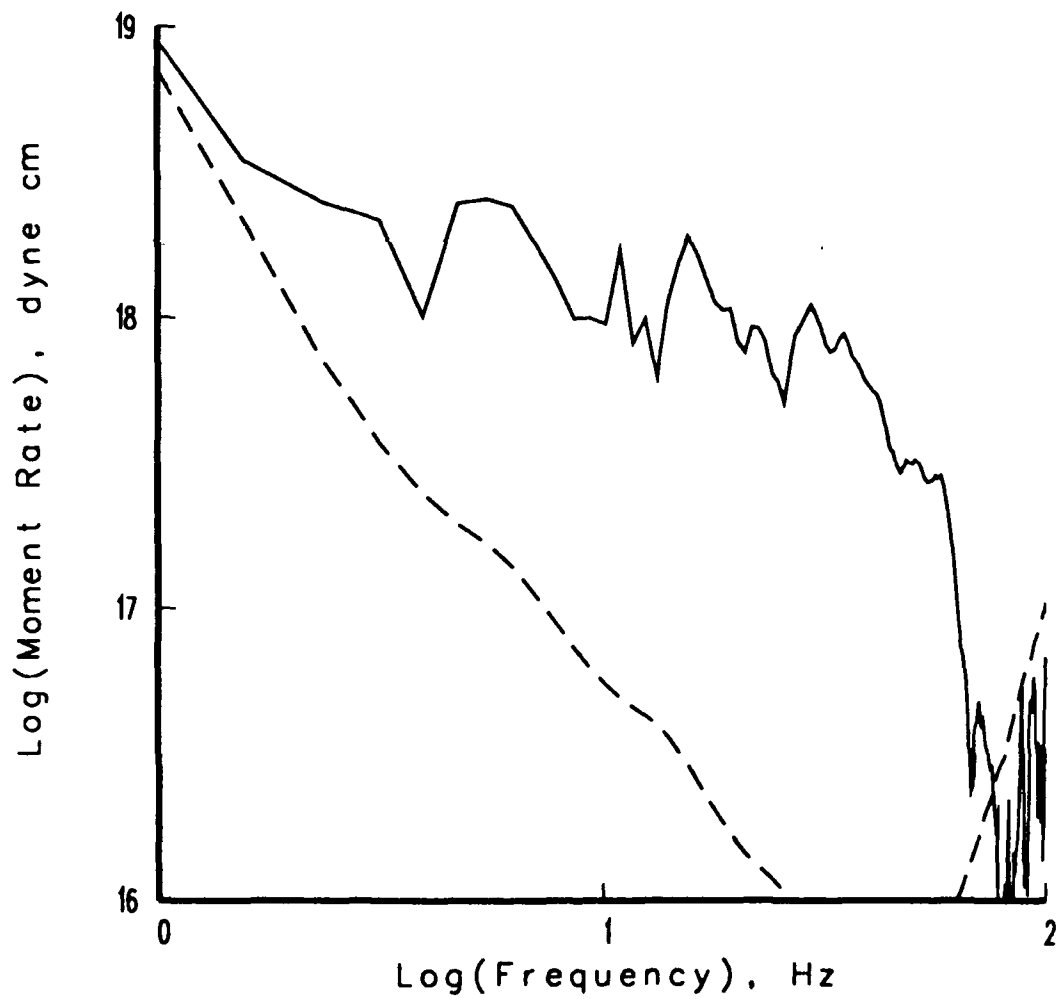


Figure 33. Amplitude density spectrum of the isotropic part of the moment rate tensor estimated for the event KQ03. The dashed line is the estimated standard error.

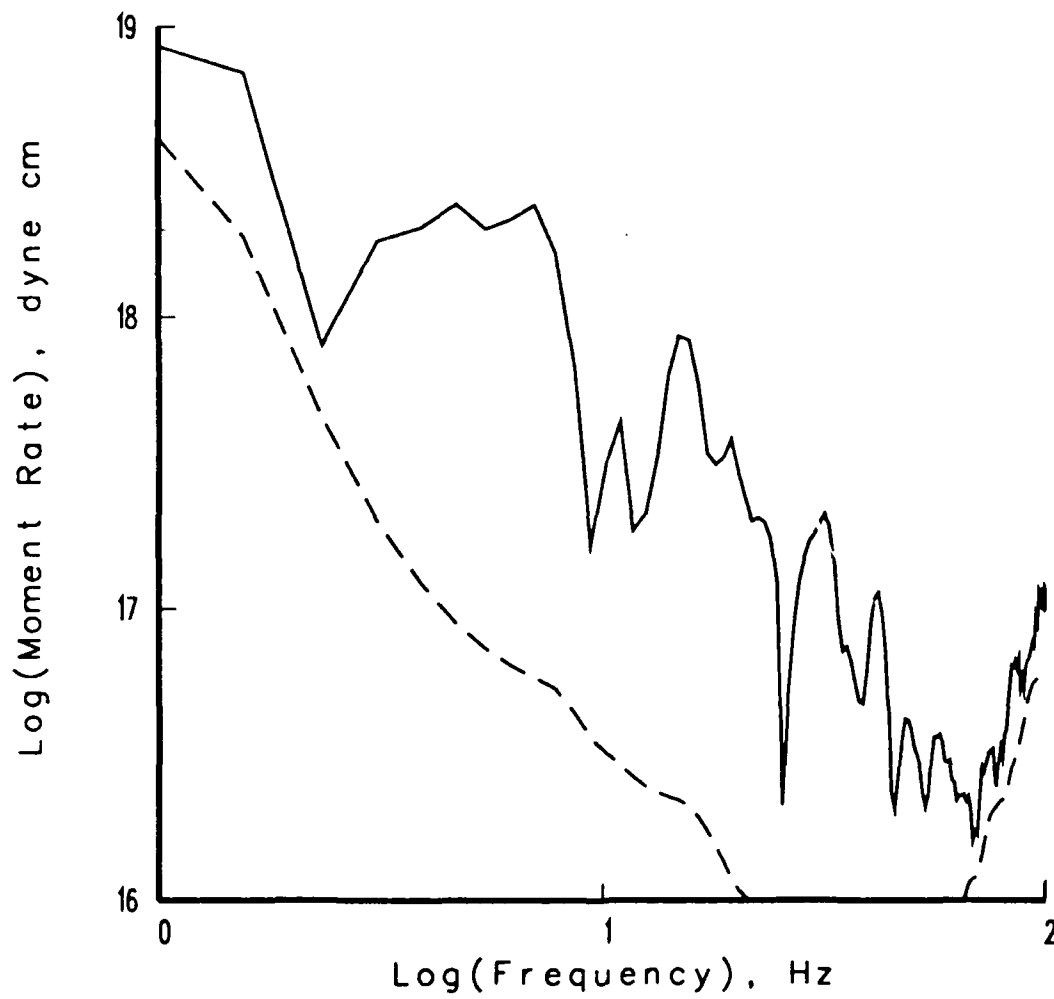


Figure 34. Amplitude density spectrum of the isotropic part of the moment rate tensor estimated for the event KQ05. The dashed line is the estimated standard error.

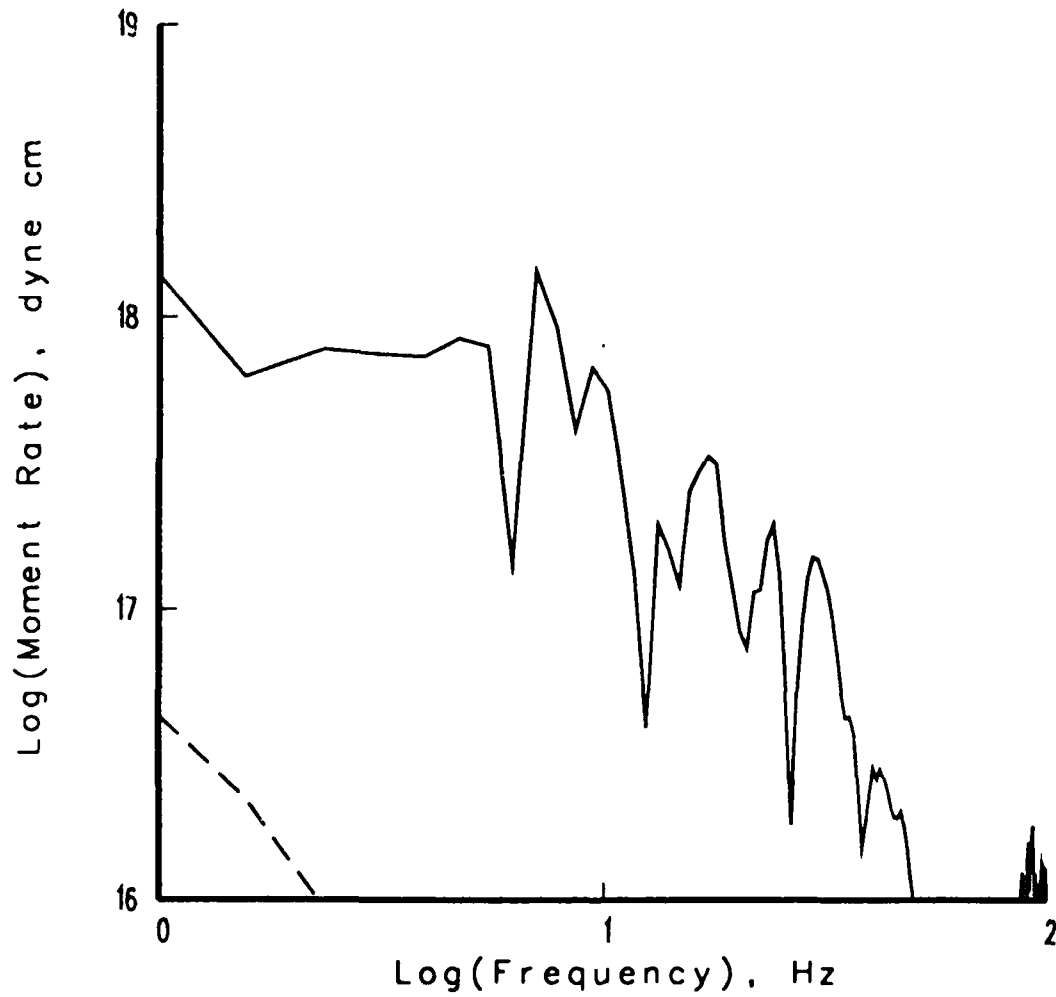


Figure 35. Amplitude density spectrum of the isotropic part of the moment rate tensor estimated for the event KQ08. The dashed line is the estimated standard error.

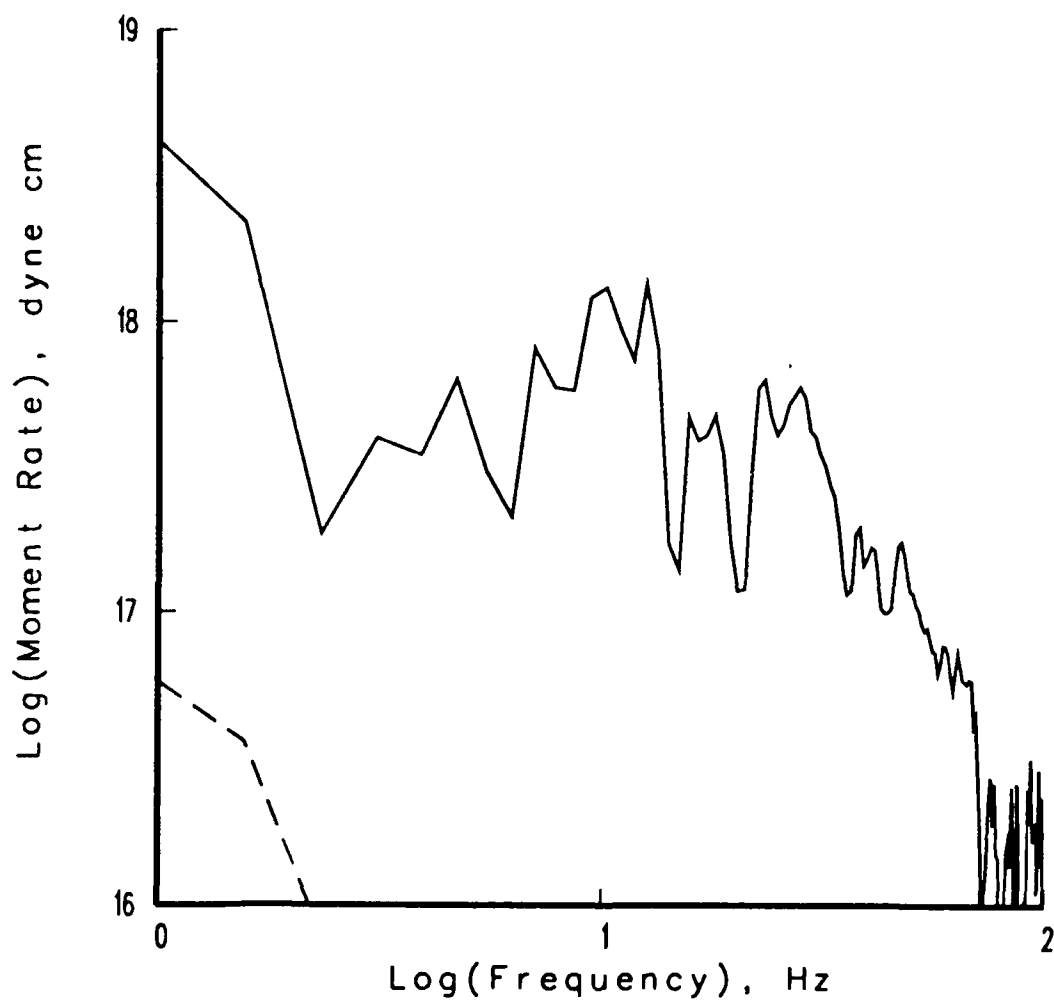


Figure 36. Amplitude density spectrum of the isotropic part of the moment rate tensor estimated for the event KQ09. The dashed line is the estimated standard error.

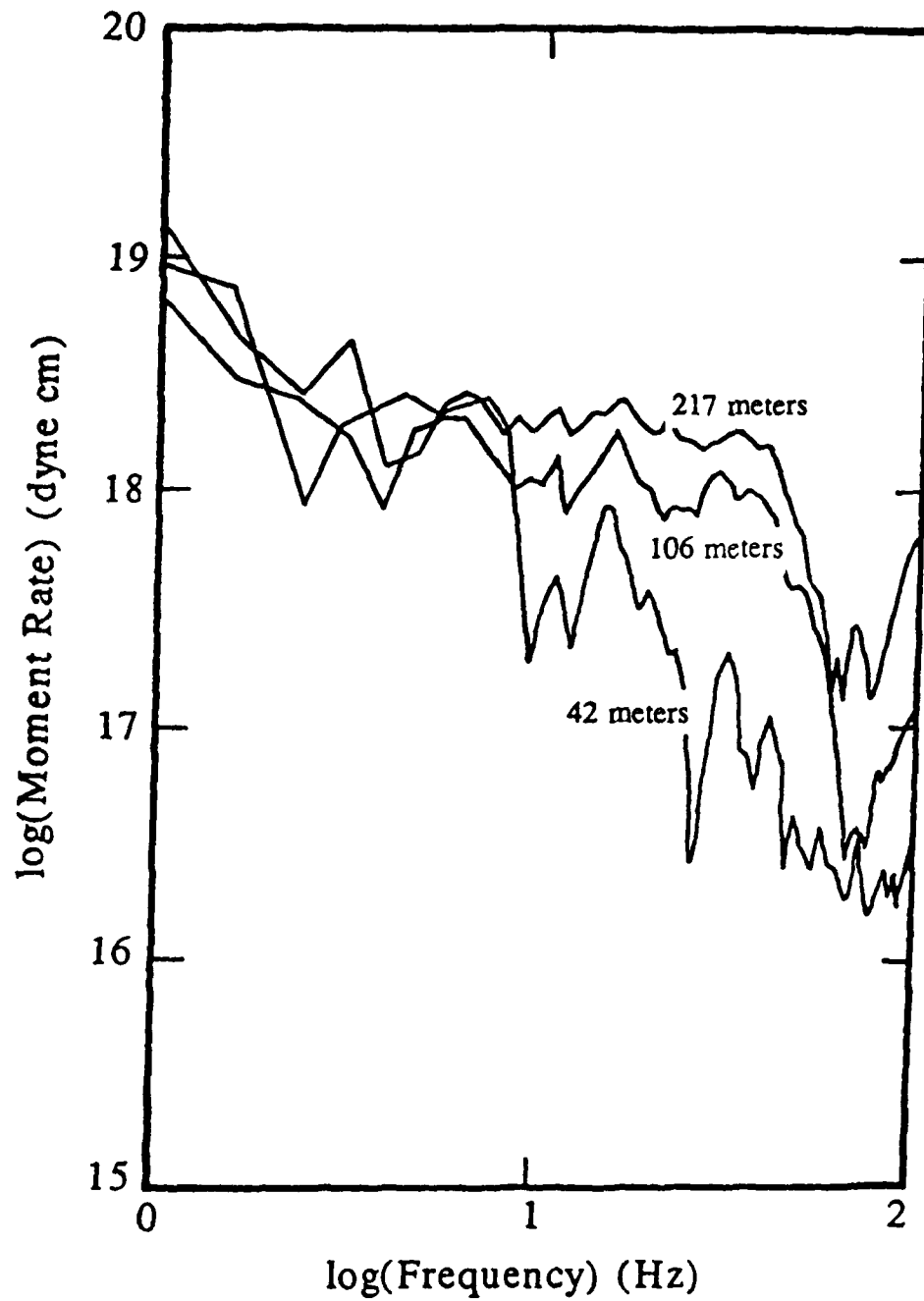


Figure 37. Comparison of the amplitude densities of the isotropic moment rate tensors for the three events in the same drilled hole, KQ01, KQ03, and KQ05. The labels on the curves are the depths of the events.

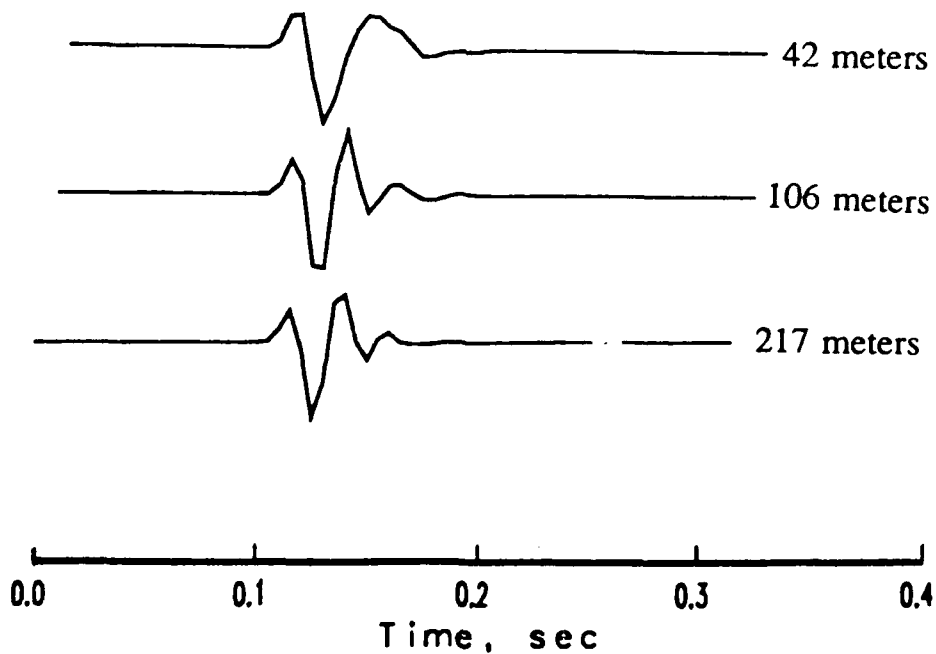


Figure 38. Comparison of the first arrival on the vertical component at station UCB3 for the three events KQ05, KQ03, and KQ01. The depth of the events are shown on the right. The pulses have been scaled to have the same amplitude on the plot, but the maximum ground accelerations for the three signals are, from the top down, 90, 293, and 393 cm/sec^2 .

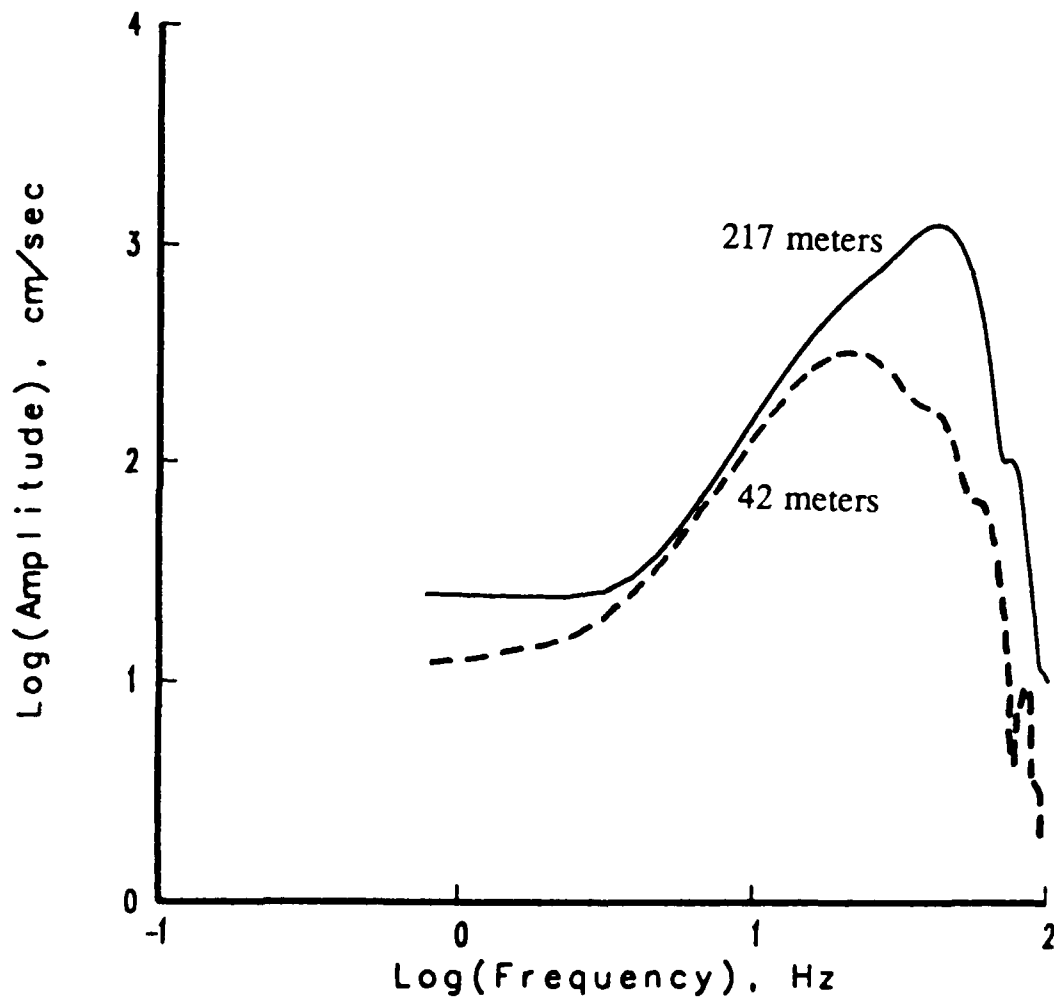


Figure 39. Amplitude density spectra of the pulses in Figure 38 for the events KQ01 and KQ05.

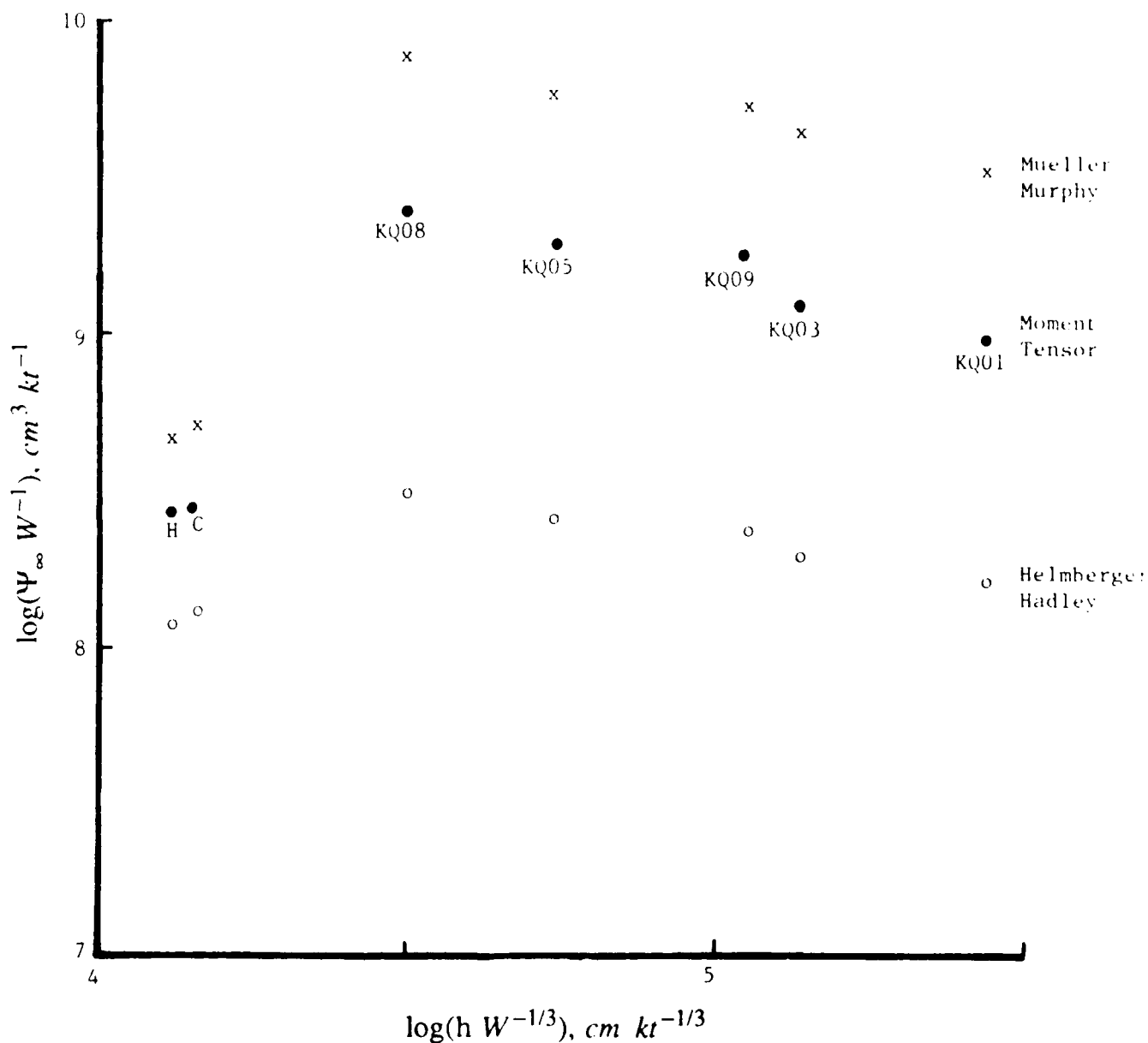


Figure 40. Scaled long time level of the reduced displacement potential of an explosion versus the scaled depth of the explosion, as determined from estimated moment tensors. The results for the five single explosions are labeled. Shown as x's are the predictions of the Mueller-Murphy scaling relationship and as o's are the predictions of the Helmberger-Hadley scaling relationship. The H and C denote results for the nuclear explosions Harzer and Chance.

CONTRACTORS (United States)

Professor Keiiti Aki
Center for Earth Sciences
University of Southern California
University Park
Los Angeles, CA 90089-0741

Professor Thomas Ahrens
Seismological Lab, 252-21
Div. of Geological & Planetary Sci.
California Institute of Technology
Pasadena, CA 91125

Professor Charles B. Archambeau
Cooperative Institute for Resch
in Environmental Sciences
University of Colorado
Boulder, CO 80309

Dr. Thomas C. Bache Jr.
Science Applications Int'l Corp.
10210 Campus Point Drive
San Diego, CA 92121 (2 copies)

Dr. Muawia Barazangi
Institute for the Study of
of the Continent
Cornell University
Ithaca, NY 14853

Dr. Douglas R. Baumgardt
Signal Analysis & Systems Div.
ENSCO, Inc.
5400 Port Royal Road
Springfield, VA 22151-2388

Dr. Jonathan Berger
IGPP, A-205
Scripps Institution of Oceanography
University of California, San Diego
La Jolla, CA 92093

Dr. S. Bratt
Science Applications Int'l Corp.
10210 Campus Point Drive
San Diego, CA 92121

Dr. Lawrence J. Burdick
Woodward-Clyde Consultants
P.O. Box 93245
Pasadena, CA 91109-3245 (2 copies)

Professor Robert W. Clayton
Seismological Laboratory/Div. of
Geological & Planetary Sciences
California Institute of Technology
Pasadena, CA 91125

Dr Karl Coyner
New England Research, Inc.
76 Olcott Drive
White River Junction, VT 05001

Dr. Vernon F. Cormier
Department of Geology & Geophysics
U-45, Room 207
The University of Connecticut
Storrs, Connecticut 06268

Dr. Steven Day
Dept. of Geological Sciences
San Diego State U.
San Diego, CA 92182

Dr. Zoltan A. Der
ENSCO, Inc.
5400 Port Royal Road
Springfield, VA 22151-2388

Professor John Ferguson
Center for Lithospheric Studies
The University of Texas at Dallas
P.O. Box 830688
Richardson, TX 75083-0688

Professor Stanley Flotte
Applied Sciences Building
University of California,
Santa Cruz, CA 95064

Dr. Alexander Florence
SRI International
333 Ravenswood Avenue
Menlo Park, CA 94025-3493

Professor Steven Grand
University of Texas at Austin
Dept of Geological Sciences
Austin, TX 78713-7909

Dr. Henry L. Gray
C.F. Frensley Professor of Mathematics
& Statistics, Vice Provost and Dean
Department of Statistical Sciences
Southern Methodist University
Dallas, TX 75275

Professor Roy Greenfield
Geosciences Department
403 Deike Building
The Pennsylvania State University
University Park, PA 16802

Dr. Indra N. Gupta
Teledyne Geotech
314 Montgomery St.
Alexandria, VA 22314

Professor David G. Harkrider
Seismological Laboratory
Div of Geological & Planetary Sciences
California Institute of Technology
Pasadena, CA 91125

Professor Donald V. Helmberger
Seismological Laboratory
Div of Geological & Planetary Sciences
California Institute of Technology
Pasadena, CA 91125

Professor Eugene Herrin
Institute for the Study of Earth
and Man/Geophysical Laboratory
Southern Methodist University
Dallas, TX 75275

Professor Robert B. Herrmann
Department of Earth & Atmospheric
Sciences
Saint Louis University
Saint Louis, MO 63156

Professor Bryan Isacks
Cornell University
Dept of Geological Sciences
SNEE Hall
Ithaca, NY 14850

Professor Lane R. Johnson
Seismographic Station
University of California
Berkeley, CA 94720

Professor Thomas H. Jordan
Department of Earth, Atmospheric
and Planetary Sciences
Mass Institute of Technology
Cambridge, MA 02139

Dr. Alan Kafka
Department of Geology &
Geophysics
Boston College
Chestnut Hill, MA 02167

Professor Leon Knopoff
University of California
Institute of Geophysics
& Planetary Physics
Los Angeles, CA 90024

Professor Charles A. Langston
Geosciences Department
403 Deike Building
The Pennsylvania State University
University Park, PA 16802

Professor Thorne Lay
Department of Geological Sciences
1006 C.C. Little Building
University of Michigan
Ann Arbor, MI 48109-1063

Dr. Randolph Martin III
New England Research, Inc.
76 Olcott Drive
White River Junction, VT 05001

Dr. Gary McCartor
Mission Research Corp.
735 State Street
P.O. Drawer 719
Santa Barbara, CA 93102 (2 copies)

Professor Thomas V. McEvilly
Seismographic Station
University of California
Berkeley, CA 94720

Dr. Keith L. McLaughlin
S-CUBED,
A Division of Maxwell Laboratory
P.O. Box 1620
La Jolla, CA 92038-1620

Professor William Menke
Lamont-Doherty Geological Observatory
of Columbia University
Palisades, NY 10964

Dr. Bernard Minster
ICPP, A-205
Scripps Institute of Oceanography
Univ. of California, San Diego
La Jolla, CA 92093

Professor Brian J. Mitchell
Department of Earth & Atmospheric
Sciences
Saint Louis University
Saint Louis, MO 63156

Mr. Jack Murphy
S-CUBED, A Division of Maxwell Lab
11800 Sunrise Valley Drive
Suite 1212
Reston, VA 22091 (2 copies)

Dr. Bao Nguyen
GL/LWH
Hanscom AFB, MA 01731-5000

Professor J. A. Orcutt
IGPP, A-205
Scripps Institute of Oceanography
Univ. of California, San Diego
La Jolla, CA 92093

Professor Keith Priestley
University of Nevada
Mackay School of Mines
Reno, NV 89557

Professor Paul G. Richards
Lamont-Doherty Geological
Observatory of Columbia Univ.
Palisades, NY 10964

Wilmer Rivers
Teledyne Geotech
314 Montgomery Street
Alexandria, VA 22314

Dr. Alan S. Ryall, Jr.
Center of Seismic Studies
1300 North 17th Street
Suite 1450

Arlington, VA 22209-2308 (4 copies) Ray Willeman

Professor Charles G. Sammis
Center for Earth Sciences
University of Southern California
University Park
Los Angeles, CA 90089-0741

Professor Christopher H. Scholz
Geological Sciences
Lamont-Doherty Geological Observatory
Palisades, NY 10964

Dr. Jeffrey L. Stevens
S-CUBED,
A Division of Maxwell Laboratory
P.O. Box 1620
La Jolla, CA 92038-1620

Professor Brian Stump
Institute for the Study of Earth & Man
Geophysical Laboratory
Southern Methodist University
Dallas, TX 75275

Professor Ta-Liang Teng
Center for Earth Sciences
University of Southern California
University Park
Los Angeles, CA 90089-0741

Dr. Clifford Thurber
University of Wisconsin - Madison
Dept. of Geology & Geophysics
1215 West Dayton St.
Madison, WI 53706

Professor M. Nafi Toksoz
Earth Resources Lab
Massachusetts Institute of Technology
42 Carleton Street
Cambridge, MA 02142

Professor Terry C. Wallace
Department of Geosciences
Building #77
University of Arizona
Tucson, AZ 85721

Weidlinger Associates
ATTN: Dr. Gregory Wojcik
4410 El Camino Real, Suite 110
Los Altos, CA 94022

GL/LWH
Hanscom AFB, MA 01731-5000

Dr. Lorraine Wolfe
GL/LWH
Hanscom AFB, MA 01731-5000

Professor Francis T. Wu
Department of Geological Sciences
State University of New York
at Binghamton
Vestal, NY 13901

OTHERS (United States)

Dr. Monem Abdel-Gawad
Rockwell Internat'l Science Center
1049 Camino Dos Rios
Thousand Oaks, CA 91360

Professor Shelton S. Alexander
Geosciences Department
403 Deike Building
The Pennsylvania State University
University Park, PA 16802

Dr. Ralph Archuleta
Department of Geological Sciences
Univ. of California at
Santa Barbara
Santa Barbara, CA

J. Barker
Department of Geological Sciences
State University of New York
at Binghamton
Vestal, NY 13901

Mr. William J. Best
907 Westwood Drive
Vienna, VA 22180

Dr. N. Biswas
Geophysical Institute
University of Alaska
Fairbanks, AK 99701

Dr. G. A. Bollinger
Department of Geological Sciences
Virginia Polytechnical Institute
21044 Derring Hall
Blacksburg, VA 24061

Mr. Roy Burger
1221 Serry Rd.
Schenectady, NY 12309

Dr. Robert Burrige
Schlumberger-Doll Resch Ctr.
Old Quarry Road
Middletown, CT 06877

Science Horizons, Inc.
ATTN: Dr. Theodore Cherry
710 Encinitas Blvd., Suite 200
Encinitas, CA 92024 (2 copies)

Professor Jon F. Claerbout
Professor Amos Nur
Dept. of Geophysics
Stanford University
Stanford, CA 94305 (2 copies)

Dr. Anton W. Dainty
Earth Resources Lab
Massachusetts Institute of Technology
42 Carleton Street
Cambridge, MA 02142

Professor Adam Dzierwonski
Hoffman Laboratory
Harvard University
20 Oxford St.
Cambridge, MA 02138

Professor John Ebel
Dept of Geology and Geophysics
Boston College
Chestnut Hill, MA 02167

Dr. Donald Forsyth
Dept of Geological Sciences
Brown University
Providence, RI 02912

Dr. Anthony Gangl
Texas A&M University
Department of Geophysics
College Station, TX 77843

Dr. Freeman Gilbert
Inst. of Geophysics & Planetary Physics
University of California, San Diego
P.O. Box 109
La Jolla, CA 92037

Mr. Edward Giller
Pacific Seirra Research Corp.
1401 Wilson Boulevard
Arlington, VA 22209

Dr. Jeffrey W. Given
Sierra Geophysics
11255 Kirkland Way
Kirkland, WA 98033

Rong Song Jih
Teledyne Geotech
314 Montgomery Street
Alexandria, VA 22314

Professor F.K. Lamb
Univ. of Illinois at Urbana-Champaign
Department of Physics
1110 West Green Street
Urbana, IL 61801

Dr. Arthur Lerner-Lam
Lamont-Doherty Geological Observatory
of Columbia University
Palisades, NY 10964

Dr. L. Timothy Long
School of Geophysical Sciences
Georgia Institute of Technology
Atlanta, GA 30332

Dr. Peter Malin
University of California at
Santa Barbara
Institute for Central Studies
Santa Barbara, CA 93106

Dr. George R. Mellman
Sierra Geophysics
11255 Kirkland Way
Kirkland, WA 98033

Professor John Nabelek
College of Oceanography
Oregon State University
Corvallis, OR 97331

Dr. Geza Nagy
U. California, San Diego
Dept of Ames, M.S. B-010
La Jolla, CA 92093

Dr. Jack Oliver
Department of Geology
Cornell University
Ithaca, NY 14850

Dr. Robert Phinney/Dr. F. A. Dahlen
Dept of Geological
Geological Science University
Princeton University
Princeton, NJ 08540

RADIX System, Inc.
Attn: Dr. Jay Pulli
2 Taft Court, Suite 203
Rockville, Maryland 20850

Dr. Norton Rimer
S-CUBED
A Division of Maxwell Laboratory
P.O. 1620
La Jolla, CA 92038-1620

Professor Larry J. Ruff
Department of Geological Sciences
1006 C.C. Little Building
University of Michigan
Ann Arbor, MI 48109-1063

Dr. Richard Sailor
TASC Inc.
55 Walkers Brook Drive
Reading, MA 01867

Thomas J. Sereno, Jr.
Science Application Int'l Corp.
10210 Campus Point Drive
San Diego, CA 92121

Dr. David G. Simpson
Lamont-Doherty Geological Observ.
of Columbia University
Palisades, NY 10964

Dr. Bob Smith
Department of Geophysics
University of Utah
1400 East 2nd South
Salt Lake City, UT 84112

Dr. S. W. Smith
Geophysics Program
University of Washington
Seattle, WA 98195

Dr. Stewart Smith
IRIS Inc.
1616 N. Fort Myer Dr.
Suite 1440
Arlington, VA 22209

Rondout Associates
ATTN: Dr. George Sutton,
Dr. Jerry Carter, Dr. Paul Pomeroy
P. O. Box 224
Stone Ridge, NY 12484 (4 copies)

Dr. L. Sykes
Lamont Doherty Geological Observ.
Columbia University
Palisades, NY 10964

Dr. Pradeep Talwani
Department of Geological Sciences
University of South Carolina
Columbia, SC 29208

Dr. R. B. Tittmann
Rockwell International Science Center
1049 Camino Dos Rios
P.O. Box 1085
Thousand Oaks, CA 91360

Dr. Gregory van der Vink
IRIS, Inc.
1616 No. Fort Myer Drive
Suite 1440
Arlington, VA 22209

Professor John H. Woodhouse
Hoffman Laboratory
Harvard University
20 Oxford St.
Cambridge, MA 02138

Dr. Gregory B. Young
ENSCO, Inc.
5400 Port Royal Road
Springfield, VA 22151-2388

FOREIGN (OTHERS)

Dr. Peter Basham
Earth Physics Branch
Geological Survey of Canada
1 Observatory Crescent
Ottawa, Ontario, CANADA K1A 0Y3

Professor Ari Ben-Menahem
Dept of Applied Mathematics
Weizman Institute of Science
Rehovot
ISRAEL 951729

Dr. Eduard Berg
Institute of Geophysics
University of Hawaii
Honolulu, HI 96822

Dr. Michel Bouchon
I.R.I.G.M.-B.P.
38402 St. Martin D'Heres
Cedex FRANCE

Dr. Hilmar Bungum/NTNF/NORSAR
P.O. Box 51
Norwegian Council of Science,
Industry and Research, NORSAR
N-2007 Kjeller, NORWAY

Dr. Michel Campillo
I.R.I.G.M.-B.P. 68
38402 St. Martin D'Heres
Cedex, FRANCE

Dr. Kin-Yip Chun
Geophysics Division
Physics Department
University of Toronto
Ontario, CANADA M5S 1A7

Dr. Alan Douglas
Ministry of Defense
Blacknest, Brimpton,
Reading RG7-4RS
UNITED KINGDOM

Dr. Manfred Henger
Fed. Inst. For Geosciences & Nat'l Res.
Postfach 510153
D-3000 Hannover 51
FEDERAL REPUBLIC OF GERMANY

Ms. Eva Johannisson
Senior Research Officer
National Defense Research Inst.
P.O. Box 27322
S-102 54 Stockholm, SWEDEN

Tormod Kvaerna
NTNF/NORSAR
P.O. Box 51
N-2007 Kjeller, NORWAY

Mr. Peter Marshall, Procurement
Executive, Ministry of Defense
Blacknest, Brimpton,
Reading RG7-4RS
UNITED KINGDOM (3 copies)

Dr. Robert North
Geophysics Division
Geological Survey of Canada
1 Observatory crescent
Ottawa, Ontario, CANADA K1A 0Y3

Dr. Frode Ringdal
NTNF/NORSAR
P.O. Box 51
N-2007 Kjeller, NORWAY

Dr. Jorg Schlittenhardt
Fed. Inst. for Geosciences & Nat'l Res.
Postfach 510153
D-3000 Hannover 51
FEDERAL REPUBLIC OF GERMANY

University of Hawaii
Institute of Geophysics
ATTN: Dr. Daniel Walker
Honolulu, HI 96822

FOREIGN CONTRACTORS

Dr. Ramon Cabre, S.J.
Observatorio San Calixto
Castilla 5939
La Paz Bolivia

Professor Peter Harjes
Institute for Geophysik
Rhur University/Bochum
P.O. Box 102148, 4630 Bochum 1
FEDERAL REPUBLIC OF GERMANY

Dr. E. Husebye
NTNF/NORSAR
P.O. Box 51
N-2007 Kjeller, NORWAY

Professor Brian L.N. Kennett
Research School of Earth Sciences
Institute of Advanced Studies
G.P.O. Box 4
Canberra 2601, AUSTRALIA

Dr. B. Massinon
Societe Radiomana
27, Rue Claude Bernard
75005, Paris, FRANCE (2 copies)

Dr. Pierre Mechler
Societe Radiomana
27, Rue Claude Bernard
75005, Paris, FRANCE

Dr. Svein Mykkeltveit
NTNF/NORSAR
P.O. Box 51
N-2007 Kjeller, NORWAY (3 copies)

GOVERNMENT

Dr. Ralph Alewine III
DARPA/NMRO
1400 Wilson Boulevard
Arlington, VA 22209-2308

James C. Rattis
GL/LWH
Hanscom AFB, MA 01731-5000

Dr. Robert Blandford
DARPA/NMRO
1400 Wilson Boulevard
Arlington, VA 22209-2308

Dr. John J. Cipar
GL/LWH
Hanscom AFB, MA 01731-5000

Sandia National Laboratory
ATTN: Dr. H. R. Durham
Albuquerque, NM 87185

Dr. Jack Evernden
USGS-Earthquake Studies
345 Middlefield Road
Menlo Park, CA 94025

U.S. Geological Survey
ATTN: Dr. T. Hanks
Nat'l Earthquake Resch Center
345 Middlefield Road
Menlo Park, CA 94025

Dr. James Hannon
Lawrence Livermore Nat'l Lab.
P.O. Box 808
Livermore, CA 94550

Neil Johnson
ESS-4, Mail Stop J979
Los Alamos National Laboratory
Los Alamos, NM 87545

Janet Johnston
GL/LWH
Hanscom AFB, MA 01731-5000

Dr. Katherine Kadinsky-Cade
GL/LWH
Hanscom AFB, MA 01731-5000

Ms. Ann Kerr
IGPP, A-205
Scripps Institute of Oceanography
Univ. of California, San Diego
La Jolla, CA 92093

Dr. Max Koontz
US Dept of Energy/DP 5
Forrestal Building
1000 Independence Ave.
Washington, D.C. 20585

Dr. W. H. K. Lee
Office of Earthquakes, Volcanoes,
& Engineering
345 Middlefield Rd
Menlo Park, CA 94025

Dr. William Leith
U.S. Geological Survey
Mail Stop 928
Reston, VA 22092

Dr. Richard Lewis
Dir. Earthquake Engrg & Geophysics
U.S. Army Corps of Engineers
Box 631
Vicksburg, MS 39180

James F. Lewkowicz
GL/LWH
Hanscom AFB, MA 01731-5000

Stephen Mangino
GL/LWH
Hanscom AFB, MA 01731-5000

Dr. Robert Masse
Box 25046, Mail Stop 967
Denver Federal Center
Denver, CO 80225

Richard Morrow
ACDA/VI
Room 5741
320 21st Street N.W.
Washington, D.C. 20451

Dr. Keith K. Nakanishi
Lawrence Livermore National Laboratory
P.O. Box 808, L-205
Livermore, CA 94550 (2 copies)

Dr. Carl Newton
Los Alamos National Lab.
P.O. Box 1663
Mail Stop C335, Group ESS-3
Los Alamos, NM 87545

Dr. Kenneth H. Olsen
Los Alamos Scientific Lab.
P.O. Box 1663
Mail Stop C335, Group ESS-3
Los Alamos, NM 87545

Howard J. Patton
Lawrence Livermore National Laboratory
P.O. Box 808, L-205
Livermore, CA 94550

Mr. Chris Paine
Office of Senator Kennedy
SR 315
United States Senate
Washington, D.C. 20510

AFOSR/NP
ATTN: Colonel Jerry J. Perrizo
Bldg 410
Bolling AFB, Wash D.C. 20332-6448

HQ AFTAC/TT
Attn: Dr. Frank F. Pilotte
Patrick AFB, Florida 32925-6001

Mr. Jack Rachlin
USGS - Geology, Rm 3 C136
Mail Stop 928 National Center
Reston, VA 22092

Robert Reinke
AFWL/NTEG
Kirtland AFB, NM 87117-6008

Dr. Byron Ristvet
HQ DNA, Nevada Operations Office
Attn: NVCG
P.O. Box 98539
Las Vegas, NV 89193

HQ AFTAC/TGR
Attn: Dr. George H. Rothe
Patrick AFB, Florida 32925-6001

Donald L. Springer
Lawrence Livermore National Laboratory
P.O. Box 808, L-205
Livermore, CA 94550

Dr. Lawrence Turnbull
OSWR/NED
Central Intelligence Agency
CIA, Room 5G48
Washington, D.C. 20505

Dr. Thomas Weaver
Los Alamos National Laboratory
P.O. Box 1663
MS C 335
Los Alamos, NM 87545

GL/SULL
Research Library
Hanscom AFB, MA 01731-5000 (2 copies)

Secretary of the Air Force (SAFRD)
Washington, DC 20330
Office of the Secretary Defense
DDR & E
Washington, DC 20330

HQ DNA
ATTN: Technical Library
Washington, DC 20305

DARPA/RMO/RETRIEVAL
1400 Wilson Blvd.
Arlington, VA 22209

DARPA/RMO/Security Office
1400 Wilson Blvd.
Arlington, VA 22209

GL/XO
Hanscom AFB, MA 01731-5000

GL/LW
Hanscom AFB, MA 01731-5000

DARPA/PM
1400 Wilson Boulevard
Arlington, VA 22209

Defense Technical
Information Center
Cameron Station
Alexandria, VA 22314
(5 copies)

Defense Intelligence Agency
Directorate for Scientific &
Technical Intelligence
Washington, D.C. 20301

Defense Nuclear Agency/SPSS
ATTN: Dr. Michael Shore
6801 Telegraph Road
Alexandria, VA 22310

AFTAC/CA (STINFO)
Patrick AFB, FL 32925-6001

Mr. Alfred Lieberman
ACDA/VI-0A'State Department Building
Room 5726
320 - 21st Street, NW
Washington, D.C. 20451

TACTEC
Rattelle Memorial Institute
505 King Avenue
Columbus, OH 43201 (Final report only)